

Confined Phase In The Real Time Formalism And The Fate Of The World Behind The Horizon

FURUUCHI Kazuyuki

*Harish-Chandra Research Institute
Chhatnag Road, Jhusi, Allahabad 211 019, India
furuuchi@mri.ernet.in*

Abstract

In the real time formulation of finite temperature field theories, one introduces an additional set of fields (type-2 fields) associated to each field in the original theory (type-1 field). In [1], in the context of the AdS-CFT correspondence, Maldacena interpreted type-2 fields as living on a boundary behind the black hole horizon. However, below the Hawking-Page transition temperature, the thermodynamically preferred configuration is the thermal AdS without a black hole, and hence there are no horizon and boundary behind it. This means that when the dual gauge theory is in confined phase, the type-2 fields cannot be associated with the degrees of freedom behind the black hole horizon. I argue that in this case the role of the type-2 fields is to make up *bulk* type-2 fields of classical closed string field theory on AdS at finite temperature in the real time formalism.

Contents

1	Introduction	1
2	Perturbative method in confined phase in the real time formalism	5
2.1	Perturbative method in the real time formalism	5
2.2	Incorporating the effect of confined phase background	8
3	Analysis of Feynman diagrams in the confined phase	11
3.1	Diagrams which have an index loop with only one cut – vanish	13
3.2	The case in which a cut-out loop divides a diagram into two disconnected pieces, one of which does not contain the external legs – still vanish	14
3.3	The case in which every cut-out loop divides a diagram into two disconnected pieces both containing the external legs – some diagrams survive . . .	18
4	Surviving diagrams as closed string tree diagrams in the real time formulation in the bulk	19
4.1	Cut-out loops as cuts of closed string propagators	20
4.1.1	An isolated cut-out loop	20
4.1.2	Closed circuits as overlapping cut-out loops	23
4.2	Closed string interaction vertices	28
5	Summary and Discussions	30
A	A sample calculation	34
A.1	Only one cut on an index loop	37
A.2	The case in which a cut-out loop divides the diagram into two pieces both containing an external leg	38
A.2.1	The vanishing case	39
A.2.2	The non-vanishing case	40

1 Introduction

The AdS-CFT correspondence [2] has provided us with powerful tools to tackle the puzzles surrounding black holes in asymptotically Anti-de Sitter (AdS) spaces. Strong evi-

dences for correspondence between deconfinement phase transition in gauge theory and Hawking-Page transition to black hole geometry [3] have been given in [4, 5] in the Euclidean path integral formulation of finite temperature field theory [6, 7] (also referred to as imaginary time formalism). Again in the imaginary time formalism, the author recently showed how the expectation value of the Polyakov loop, the order parameter of confinement-deconfinement transition, encodes the dual bulk geometry in correlation functions of gauge invariant operators [8].¹ However, the real problems about black holes, such as the information loss paradox, dynamical formation and evaporation of black holes, causal structure and singularities, can only be studied in the Lorentzian signature.

In the real time formulation of finite temperature field theories [11, 12, 13, 14, 15],² it seems unavoidable to introduce an additional set of fields besides the original ones (those in the zero-temperature theory). Each of the newly introduced field is associated with a field in the original theory. (In this article I will call newly introduced fields as type-2 fields, as opposed to the original fields which I will call type-1 fields.) On the other hand, the extended Carter-Penrose diagram of the AdS-Schwarzshild black hole geometry has a boundary behind the horizon (Fig.1 boundary 2), in addition to the usual boundary of the AdS space at spatial infinity outside the horizon (Fig.1 boundary 1). In [1], in the context of the AdS-CFT correspondence, Maldacena identified the type-2 fields as living³ on the boundary behind the black hole horizon.⁴ This gives a nice explanation for the necessity of the introduction of type-2 fields in the real time formulation of the finite temperature field theory.⁵

However, there is a small puzzle here: Below the Hawking-Page transition temperature, the thermodynamically preferred configuration in canonical ensemble is the thermal AdS

¹See also [9] for further investigation on some aspects of the confined phase in large N gauge theories in the imaginary time formalism, and [10] for its relation to the large N reductions.

²See [14] and a review [16] for the real time formulation of finite temperature field theories relevant for this article.

³The word “living” here is used metaphorically, and the role of type-2 fields in the dual bulk geometry should be made more precise by further study. This is one of the purposes of this paper. See also [18] for a related study.

⁴That the eternal black hole in AdS space is related to an entangled state in the CFT was observed in [19, 20].

⁵A description of the thermodynamical nature of black holes by thermo field dynamics was studied in [21] in early days. For further investigations after [1] see [22, 17]. For recent studies with more emphasis on the real time formalism, which is closer to the interest of this article, see [18, 23].

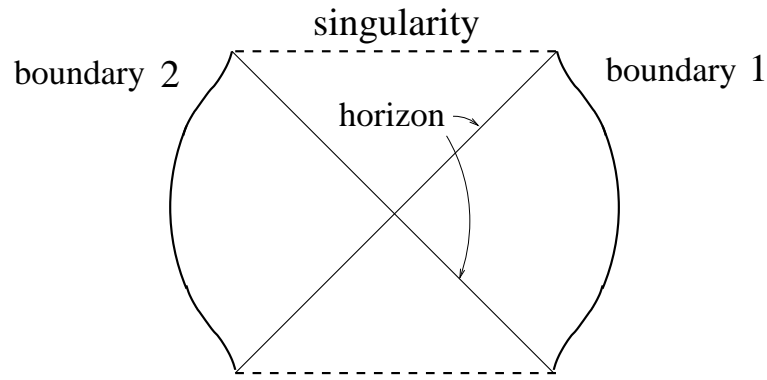


Figure 1: The extended Carter-Penrose diagram of the AdS-Schwarzschild black hole geometry. Spherical directions are suppressed in the figure. Besides the usual boundary of the AdS space at spatial infinity (boundary 1, see also Fig.2), there is a second boundary behind the horizon (boundary 2). For a more detail, see e.g. [17].

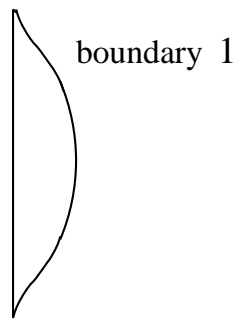


Figure 2: A Carter-Penrose diagram of the AdS geometry.

without a black hole [3]. Since it is a finite temperature system, the dual gauge theory should still be described by the real time formulation for the finite temperature. Thus one must conclude that below the Hawking-Page transition temperature, the type-2 fields in the dual gauge theory cannot correspond to the degrees of freedom behind the black hole horizon, since there is no black hole at all. But then, what is the dual bulk description for the type-2 fields in this case? Since the AdS geometry corresponds to the confined phase in gauge theory side, confinement should change the role of the type-2 fields in the bulk. In this article, I will show that this is indeed the case. In the confined phase, the role of type-2 fields in the gauge theory is to make up *bulk* type-2 fields of closed string field theory on AdS at finite temperature in the real time formalism. Since the bulk is also at finite temperature, it is very natural that the bulk theory also has type-2 fields of its own. The discussions will be in the leading order in the $1/N$ expansion, which corresponds to the classical theory in the bulk. Since the Carter-Penrose diagram is based on classical gravity,⁶ this is sufficient to explain the non-existence of the world behind the horizon in this case.

An outline of the organization of this article is as follows: In section 2, I review the derivation of Feynman rules in the real time formulation of field theories at finite temperature. Then, I give a crucial prescription for incorporating the effect of confined phase background in this formalism. In section 3, I study Feynman diagrams in large N gauge theories in the confined phase and show a large class of them vanish. To illustrate the mechanism which selects the non-vanishing diagrams, a simple example is given in Appendix A. In section 4, I argue that the surviving Feynman diagrams can be interpreted as tree diagrams of closed string field theory on AdS at finite temperature in the real time formalism. Section 5 is devoted to summary and discussions.

⁶In this article the term “gravity” will be used with possible α' corrections in mind. In other words, I assume that gravity has its origin in closed string theory. I also expect, as in [24, 25], that the Hawking-Page transition observed in the Einstein-Hilbert action (the lowest order in the α' expansion) continuously extends to its α' corrected version all down to the string scale curvature regime, which is dual to the weakly coupled gauge theory.

2 Perturbative method in confined phase in the real time formalism

2.1 Perturbative method in the real time formalism

In this section, I will review the perturbative method⁷ in the real time formulation of finite temperature field theories coupled to a gauge field. A concrete example in mind is the $\mathcal{N} = 4$ super Yang-Mills theory with $SU(N)$ gauge group on S^3 in the 't Hooft limit [4, 5, 26, 27, 24], but the method itself is applicable to general gauge theories in the 't Hooft limit. To illustrate the point, I take a real scalar field $\Phi_{ab}(t)$ in the adjoint representation of $SU(N)$ as an example. Here, a, b are $SU(N)$ gauge indices. It is straightforward to include several scalar fields, fermions or dynamical gauge fields. Since I am interested in the low temperature confined phase, it is sufficient to study quantum mechanics obtained by dimensional reduction of spatial coordinates on S^3 . (This approximation is valid when the inverse temperature β and the length scale of interest are much larger than the radius of the S^3 .) It is not difficult to generalize the discussion to more general spatial manifolds, not necessarily with dimensional reductions, by replacing the mass in the discussions below to the eigenvalues of the spatial Laplacian. The quantities of interest are thermal Green's functions $G_\beta(t_1, \dots, t_n)$ of the time-ordered products⁸ of operators $\hat{\Phi}(t)$ in Heisenberg picture:

$$G_\beta(t_1, \dots, t_n) = \frac{1}{\text{Tr } e^{-\beta \hat{H}}} \text{Tr} \left\{ e^{-\beta \hat{H}} T[\hat{\Phi}(t_1) \dots \hat{\Phi}(t_n)] \right\}, \quad (2.1)$$

where “Tr” is the trace over *physical* states satisfying the Gauss' law constraints:

$$\hat{\rho}_{ab} |phys\rangle = 0. \quad (2.2)$$

Here $\hat{\rho}_{ab} = i([\hat{\Phi}, \hat{\Pi}_\Phi]_{ab})$ is the generator of the gauge transformation, where $\hat{\Pi}_{\Phi ab}$ is the conjugate momentum of $\hat{\Phi}_{ab}$. $T[\dots]$ denotes the time ordering and β is the inverse temperature. The Hamiltonian \hat{H} is given by

$$\hat{H} = \text{tr} \left\{ \frac{g^2}{2} \hat{\Pi}_\Phi \hat{\Pi}_\Phi + \frac{\omega^2}{2g^2} \hat{\Phi}^2 + \frac{1}{g^2} V[\hat{\Phi}] \right\}, \quad (2.3)$$

⁷One may feel it slightly odd to study the confined phase by perturbative method, but as mentioned above, the expectation here is that, as in [24, 25], the deconfinement phase transition observed at weak coupling persists continuously up to strong coupling.

⁸Precisely speaking, these are the so-called T^* -products since I will eventually be interested in the quantities obtained by path integral.

where g is a gauge coupling constant, “tr” is a trace over the $SU(N)$ gauge group indices and $V[\hat{\Phi}]$ is a potential term. The mass ω is proportional to the inverse radius of S^3 in the case when the quantum mechanics is obtained from the compactification of four dimensional conformal field theory on S^3 . In order to evaluate the thermal Green’s functions by the path integral method, the support of the field variables should be extended to the whole complex t -plane as in [14]:

$$\hat{\Phi}(t) = e^{i\hat{H}t}\hat{\Phi}(0)e^{-i\hat{H}t}. \quad (2.4)$$

One would like to have a functional representation for the generating functional $Z[J]$ such that:

$$G_\beta(t_1, \dots, t_n) = \frac{1}{Z(0)} \frac{1}{i^n} \frac{\delta}{\delta J(t_n)} \cdots \frac{\delta}{\delta J(t_1)} Z[J] \Big|_{J=0}. \quad (2.5)$$

The functional

$$\text{Tr} \left\{ e^{-\beta \hat{H}} T[e^{i \int_{-T}^T dt J(t) \hat{\Phi}(t)}] \right\} \quad (2.6)$$

has this property when $-T < t_i < T$. But in order to calculate the thermal Green’s function perturbatively, one should extend the t integration to a contour C on the complex plane:

$$Z[J] = \text{Tr} \left\{ e^{-\beta \hat{H}} T_C[e^{i \int_C dt J(t) \hat{\Phi}(t)}] \right\} \quad (2.7)$$

where the contour C is depicted in Fig.3. $T_C[\dots]$ denotes time-ordering along the contour C . By inserting a complete set of physical states satisfying (2.2), one arrives at the path integral representation of the generating functional $Z[J]$:

$$Z[J] = \int [\mathcal{D}_C \Phi] e^{i \int_C dt \{ \mathcal{L}[\Phi] + J(t) \Phi(t) \}}, \quad (2.8)$$

where $\mathcal{L}[\Phi]$ is the Lagrangian

$$\mathcal{L}[\Phi] = \frac{1}{g^2} \text{tr} \left\{ \frac{1}{2} D_t \Phi D_t \Phi - \frac{\omega^2}{2} \Phi^2 - V[\Phi] \right\}. \quad (2.9)$$

The covariant derivative is given by

$$(D_t \Phi)_{ab} = \partial_t \Phi_{ab} - i[A_0, \Phi]_{ab}. \quad (2.10)$$

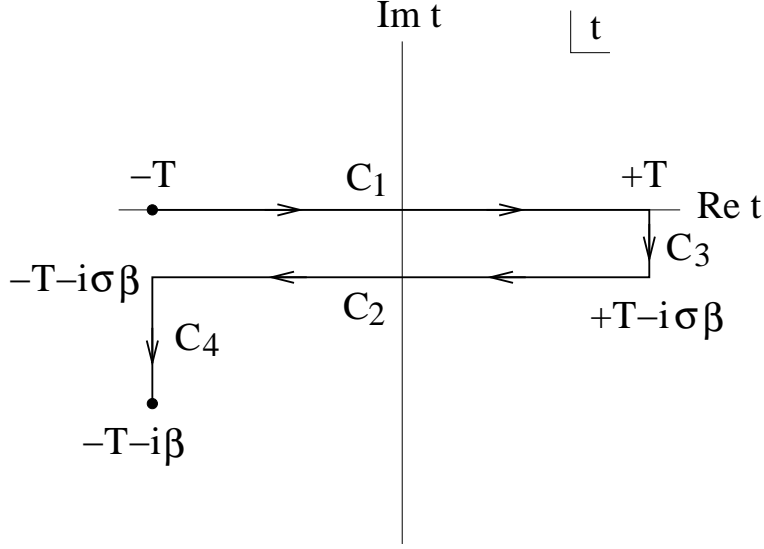


Figure 3: The contour C

The gauge field A_0 is introduced while imposing the Gauss' law constraints as delta function. The path integral is over the fields which satisfy the boundary conditions

$$\Phi_{ab}(-T - i\beta) = \Phi_{ab}(-T), \quad (2.11)$$

following from the trace over the Hilbert space in (2.1). One can rewrite (2.8) as

$$Z[J] = \exp \left\{ -i \int_C dt V \left[\frac{1}{i} \frac{\delta}{\delta J} \right] \right\} \exp \left\{ -\frac{i}{2} g^2 \int_C dt \int_C dt' J_{ab}(t) D_{ab,cd}^C(t - t') J_{cd}(t') \right\}, \quad (2.12)$$

where the thermal propagator $D_{ab,cd}^C(t - t')$ is a Green's function on the contour

$$(-\partial_t^2 - \omega^2) D_{ab,cd}^C(t - t') = \delta_C(t - t') \delta_{ad} \delta_{bc} \quad (2.13)$$

subject to the boundary condition following from (2.11). Here $\delta_C(t - t')$ is the delta function defined on the contour [14]:

$$\int_C dt \delta_C(t - t') f(t) = f(t'). \quad (2.14)$$

The boundary time T is eventually taken to infinity. By taking $J \rightarrow 0$ as $T \rightarrow \infty$, the generating functional factorizes as

$$Z[J] = Z_{12}[J] Z_{34}[J], \quad (2.15)$$

where $Z_{12}[J]$ (respectively $Z_{34}[J]$) denotes the contribution from the path C_1 and C_2 (C_3 and C_4). The effect of finite temperature enters in the propagators through the boundary condition (2.11). Although the generating functional can be seen to factorize, $Z_{34}[J]$ part plays a role for modifying the boundary conditions on the Green's function, as I will explain below.

2.2 Incorporating the effect of confined phase background

In this subsection I present a prescription for reading off the dual bulk description corresponding to the confined phase in the real time formalism. When there are no external operator insertions, one can take the Matsubara contour, i.e. the line straight down from $-T$ to $-T - i\beta$. Then the calculation reduces to that in the imaginary time formalism, where the confined phase is characterized by the vanishing of the expectation value of the Polyakov loop. The large N saddle point value of the temporal gauge field A_0 is given by

$$A_{0ab} = \delta_{ab} \frac{2\pi}{\beta N} \left(a - \frac{N+1}{2} \right) \quad (\text{constant}) \quad (2.16)$$

in an appropriate gauge.⁹ This gives an appropriate expansion point for perturbation theory on the vertical parts of the contour. In the imaginary time formalism, it was essential to expand around the saddle point of A_0 (2.16) to read off the dual bulk geometry in the confined phase [8]. I claim that *also in the real time formalism, the correct prescription for reading off the dual bulk description corresponding to the confined phase is to include the saddle point value (2.16) of A_0 into the Green's function on the vertical parts of the contour*. Thus, instead of (2.13), I use Green's function which satisfies

$$(-D_t^2 - \omega^2) D_{ab,cd}^C(t - t') = \delta_C(t - t') \delta_{ad} \delta_{bc} \quad , \quad (2.17)$$

where on the vertical parts of the contour I have included the saddle point value of A_0 (2.16) in the covariant derivative D_t .¹⁰ Since I am including the effect of the A_0 configuration (2.16) on the vertical parts of the contour, it is convenient to define the

⁹For weakly coupled gauge theories on S^3 , the low temperature phase ($\beta \gg \omega^{-1}$) is the confined phase [26, 27, 24, 25]. Above, I wrote down an action for a single scalar field for which there is no deconfinement transition at zero 't Hooft coupling. However, it is straightforward to include several scalar fields to have finite deconfinement temperature. The saddle point (2.16) is evaluated from the effective action for A_0 obtained by integrating out other massive fields, which is justified in the low temperature regime [24, 25].

¹⁰On the horizontal parts of the contour one can choose $A_0 = 0$ gauge.

field¹¹

$$\tilde{\Phi}_{ab}(t) = e^{-2\pi i \frac{a-b}{\beta N} (\text{Im } t)} \Phi_{ab}(t) \quad (2.18)$$

so that the differential equation for the Green's function $\tilde{D}^C(t-t')$ for $\tilde{\Phi}(t)$ takes the form of the ordinary one (2.13):

$$(-\partial_t^2 - \omega^2) \tilde{D}_{ab,cd}^C(t-t') = \delta_C(t-t') \delta_{ad} \delta_{bc} \quad . \quad (2.19)$$

However, the field redefinition (2.18) modifies the boundary condition (2.11) to

$$\tilde{\Phi}_{ab}(-T - i\beta) = e^{2\pi i \frac{a-b}{N}} \tilde{\Phi}_{ab}(-T). \quad (2.20)$$

One can solve (2.13) with the ansatz

$$\tilde{D}_{ab,cd}^C(t-t') = \theta_C(t-t') \tilde{D}_{ab,cd}^>(t-t') + \theta_C(t'-t) \tilde{D}_{ab,cd}^<(t-t'), \quad (2.21)$$

where $\theta_C(t-t')$ is the step function defined on the contour [14]:

$$\theta_C(t-t') = \int_C^t dt'' \delta_C(t''-t'). \quad (2.22)$$

Since from (2.8) to (2.12) the change of variable

$$\tilde{\Phi}_{ab}(t) \rightarrow \tilde{\Phi}_{ab}(t) + \int_C dt' \tilde{D}_{ab,cd}(t-t') J_{cd}(t'), \quad (2.23)$$

has been made, the boundary condition (2.20) implies

$$\tilde{D}_{ab,cd}^>(t-t' - i\beta) = e^{2\pi i \frac{a-b}{N}} \tilde{D}_{ab,cd}^<(t-t'). \quad (2.24)$$

The unique solution to (2.19) with the boundary condition (2.24) is

$$\tilde{D}^C(t-t')_{ab,cd} = \frac{-i}{2\omega} \left[(A e^{-i\omega t} + B e^{i\omega t}) \theta_C(t-t') + (C e^{-i\omega t} + D e^{i\omega t}) \theta_C(t'-t) \right] \quad (2.25)$$

with

$$\begin{aligned} A &= \frac{1}{1 - e^{-\beta\omega - 2\pi i \frac{a-b}{N}}}, & B &= \frac{e^{-\beta\omega + 2\pi i \frac{a-b}{N}}}{1 - e^{-\beta\omega + 2\pi i \frac{a-b}{N}}}, \\ C &= \frac{e^{-\beta\omega - 2\pi i \frac{a-b}{N}}}{1 - e^{-\beta\omega - 2\pi i \frac{a-b}{N}}}, & D &= \frac{1}{1 - e^{-\beta\omega + 2\pi i \frac{a-b}{N}}}. \end{aligned} \quad (2.26)$$

¹¹The reason $\text{Im } t$, rather than $-it$ which is familiar from the case with chemical potential, appears here is that A_0 has non-zero expectation value only on the vertical parts of the contour.

The Green's function (2.25) can be rewritten in the spectral representation:

$$i\tilde{D}_{ab,cd}^C(t-t') = \int_{-\infty}^{\infty} \frac{dk_0}{2\pi} e^{-ik_0(t-t')} \rho(k_0) [\theta_C(t-t') + N(k_0, a-b)] \delta_{ad} \delta_{bc} \quad , \quad (2.27)$$

where

$$\rho(k_0) = 2\pi\varepsilon(k_0) \delta(k_0^2 - \omega^2), \quad \varepsilon(k_0) = \theta(k_0) - \theta(-k_0) \quad (2.28)$$

and

$$N(k_0, a-b) = \frac{1}{e^{\beta k_0 + 2\pi i \frac{a-b}{N}} - 1}. \quad (2.29)$$

As in (2.15), the partition function factorizes. Therefore, only the propagators between the fields on the contours C_1 or C_2 need to be considered. The propagators for general σ ($0 < \sigma < 1$, where σ is given in Fig.3) are obtained as

$$\tilde{D}_{ab,cd}^{(11)}(t-t') = \tilde{D}_{ab,cd}^C(t-t'), \quad (2.30)$$

$$\tilde{D}_{ab,cd}^{(22)}(t-t') = \tilde{D}_{ab,cd}^C((t-i\sigma\beta) - (t'-i\sigma\beta)), \quad (2.31)$$

$$\tilde{D}_{ab,cd}^{(12)}(t-t') = \tilde{D}_{ab,cd}^<(t - (t' - i\sigma\beta)), \quad (2.32)$$

$$\tilde{D}_{ab,cd}^{(21)}(t-t') = \tilde{D}_{ab,cd}^>((t - i\sigma\beta) - t'). \quad (2.33)$$

Notice that the propagator takes the form of a 2×2 matrix. This means that the degrees of freedom are doubled compared with the original theory (the theory at zero temperature) [14]. The doubling of the degrees of freedom originates from the two parts of the contour C_1 and C_2 in Fig.3. $\tilde{D}^{(11)}$ (respectively $\tilde{D}^{(22)}$) is a propagator between type-1 (type-2) fields, and $\tilde{D}^{(12)}$ and $\tilde{D}^{(21)}$ are mixed propagators between type-1 and type-2 fields.

By taking $\sigma = \frac{1}{2}$ as in [14, 15], one arrives at the most symmetric expression. It is convenient to split the propagator into a temperature dependent part and an independent part. Also, at this point it is convenient to undo the field redefinition (2.18) to obtain a symmetric expression for the propagators.¹² In momentum space, they are given by

$$iD_{ab,cd}^{(rs)} = iD_{0ab,cd}^{(rs)} + iD_{\beta ab,cd}^{(rs)} \quad (r, s = 1, 2), \quad (2.34)$$

$$iD_{0ab,cd} = \delta_{ad} \delta_{bc} \begin{pmatrix} \frac{i}{k_0^2 - \omega^2 + i\epsilon} & 0 \\ 0 & \frac{-i}{k_0^2 - \omega^2 - i\epsilon} \end{pmatrix}, \quad (2.35)$$

¹²The phase appears symmetrically in (1-2) and (2-1) components of the propagator (2.36).

$$iD_{\beta ab,cd} = \delta_{ad}\delta_{bc}\pi\delta(k_0^2 - \omega^2) \times \frac{1}{e^{|\beta k_0 + 2\pi i \frac{a-b}{N}|_R} - 1} \begin{pmatrix} 1 & e^{\frac{1}{2}|\beta k_0 + 2\pi i \frac{a-b}{N}|_R} \\ e^{\frac{1}{2}|\beta k_0 + 2\pi i \frac{a-b}{N}|_R} & 1 \end{pmatrix}. \quad (2.36)$$

In the above, $|\cdots|_R$ is defined as

$$|z|_R = \begin{cases} z & (\text{Re } z > 0) \\ -z & (\text{Re } z < 0) \end{cases}, \quad (\text{Re } z \neq 0). \quad (2.37)$$

Eq.(2.37) is not defined for $\text{Re } z = 0$, but because of the on-shell delta function in (2.36) one does not need to consider that case as long as $\omega \neq 0$.¹³

Perturbative Feynman rules can be obtained just as in the conventional field theories and are sketched in Fig.4. I have adopted the 't Hooft's double-line notation [28]. (1) represents the temperature independent part of the propagator $iD_{0ab,cd}^{(rs)}$ and (2) the temperature dependent part $iD_{\beta ab,cd}^{(rs)}$. The temperature dependent part of the propagator is drawn with the “cut” line in Fig.4 (2). *This cut is one of the most important tools I will use repeatedly in the following discussions.* Type-1 fields and type-2 fields are coupled only through the propagators: The interaction vertices do not mix type-1 and type-2 fields. The interaction vertices of type-2 fields are given by the complex conjugate of those of type-1 fields:

$$i \text{tr} V_2[\Phi_{(2)}] = (i \text{tr} V_1[\Phi_{(1)}])^* \Big|_{\Phi_{(1)} \rightarrow \Phi_{(2)}}. \quad (2.38)$$

I have assumed that the potential is real.

3 Analysis of Feynman diagrams in the confined phase

In this section, with the prescription for incorporating the effect of the confined phase background (2.16) discussed in the previous section, I will show that contributions from a large class of Feynman diagrams vanish. In Appendix A, a simple example of the following discussions is provided. The reader may find it helpful to read them in parallel.

The quantities of interest in this article are the correlation functions of gauge invariant single trace local operators, which correspond to closed string states in the AdS-CFT correspondence. Throughout this article I will work in the planar limit $g \rightarrow 0, N \rightarrow \infty$

¹³In the case which the quantum mechanics is obtained from the compactification of four dimensional conformal field theory on S^3 , ω is proportional to the inverse radius of S^3 and non-zero.

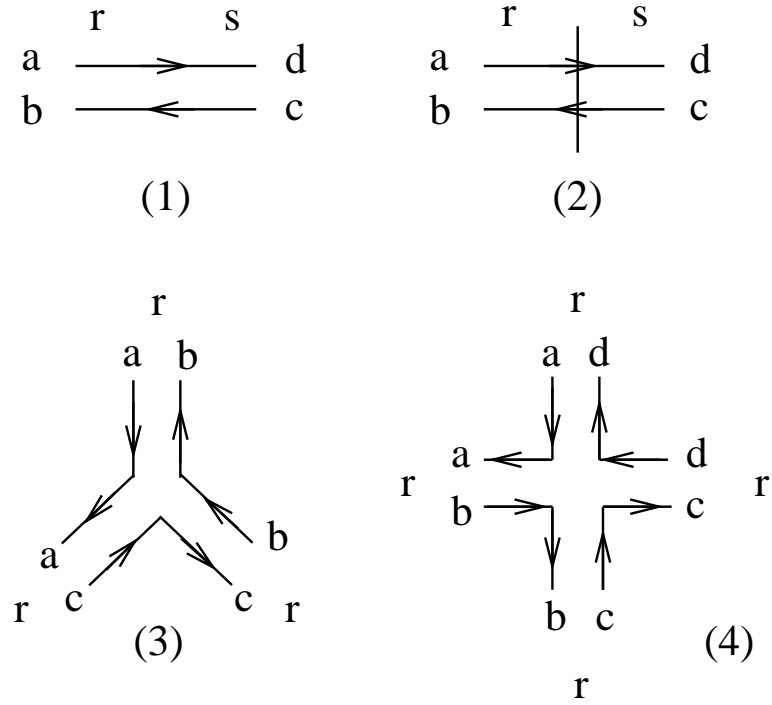


Figure 4: Feynman rules for the real time formulation of large N gauge theories at finite temperature: (1) is the temperature independent part of the propagator (2.35), while (2) is the temperature dependent part (2.36). The index flow indicated by the arrow is directed from the first matrix index to the second matrix index of adjoint fields. The temperature dependent part of the propagator (2) is drawn with a “cut” line (the vertical line in the figure). The interaction vertices (3),(4) are drawn schematically, just to show the index flow structure. One can assign a more detailed structure to the interaction vertices according to the action of one’s interest. The interaction vertices do not mix the type-1 fields with the type-2 fields.

with the 't Hooft coupling $g^2 N$ fixed. In the planar limit, one can always associate a loop momentum to an index loop [8, 10], as will be explained below.¹⁴ For a given 't Hooft-Feynman diagram, I draw a tree sub-diagram which connects the external legs, to show the flow of the external momentum (Fig.5), between the double lines. The total momentum on a propagator is a sum of two momenta associated with the index lines (taking into account the sign indicated by the arrows), and an external momentum flow if there is any. By a shift of loop momenta, which are integration variables, one can choose any tree sub-diagram connecting the external legs to express the external momentum flow. But once it is chosen, the integrations over loop momenta should be done with that fixed external momentum flow.

3.1 Diagrams which have an index loop with only one cut – vanish

I first consider Feynman diagrams which have at least one index loop containing only one cut (which is denoted as a_i below). In this case the cut must be either 1-1 or 2-2 cut.¹⁵ From (2.36), the diagram with the 1-1 or 2-2 cut is proportional to a factor

$$\sum_{a_i=1}^N \frac{1}{e^{|\beta(p_{0i}-p_{0j})+2\pi i \frac{a_i-a_j}{N}|_R} - 1}. \quad (3.1)$$

Here, i, j label the index-momentum loops. As mentioned earlier, the loop momentum p_{0i} is “associated” with the gauge index a_i , that means, they always appear in the combination $\beta p_{0i} + 2\pi i \frac{a_i}{N}$. The origin of this combination is the covariant derivative for adjoint fields. Therefore, by taking the background gauge around the field configuration (2.16), even when there are derivative couplings the loop momentum and the associated index also appear in the same combination. Such derivative couplings give rise to a multiplicative factor which is polynomial in $\beta p_{0i} + 2\pi i \frac{a_i}{N}$. Those just require a minor modification in the following discussions and do not change the conclusion about whether a diagram vanishes or not. Therefore, to keep the essential points clear in the presentation, I will only write down the formula for the case in which such derivative couplings are not involved. Since I

¹⁴There are $\ell + 1$ index loops for ℓ (momentum) loop planar diagrams of a correlation function of gauge invariant operators, but one summation over gauge indices decouples since the gauge indices always appear as a difference of two indices [8, 10].

¹⁵When there is a 1-2 cut on an index loop, there must be a 2-1 cut on that index loop. See the explanation at the end of subsection 3.3

am working in the strict $N \rightarrow \infty$ limit, the sum over the gauge indices a_i can be replaced by integral: $\frac{a_i}{N} \rightarrow \theta_i$, $\sum_{a_i=1}^N \rightarrow N \int_0^1 d\theta_i$. (To avoid repetition, this replacement will be implicit in what follows.) Then, one can Fourier expand the integrand as

$$\begin{aligned} \int_0^1 d\theta_i \frac{1}{e^{|\beta(p_{0i}-p_{0j})+2\pi i(\theta_i-\theta_j)|_R} - 1} &= \int_0^1 d\theta_i \sum_{n=1}^{\infty} e^{-n|\beta(p_{0i}-p_{0j})+2\pi i(\theta_i-\theta_j)|_R} \\ &= 0. \end{aligned} \quad (3.2)$$

From the definition (2.37), this kind of diagram has either all negative (when $p_{0i} > p_{0j}$) or all positive (when $p_{0i} < p_{0j}$) powers of $e^{2\pi i \theta_i}$. In either case, (3.2) vanishes.¹⁶ *Eq.(3.2) is the basic equation relevant for selecting non-vanishing Feynman diagrams in the confined phase, and will repeatedly appear in the following.*

3.2 The case in which a cut-out loop divides a diagram into two disconnected pieces, one of which does not contain the external legs – still vanish

In the previous subsection, I have shown that the diagrams which have an index loop with only one cut vanish. Therefore, below I will consider the cases in which all the index loops either contain no cut or more than one cut. In these cases, if there is a cut on an index loop, there must be at least one more cut on this index loop. Since the sequence of cuts cannot end on an index loop, they make up a closed circuit (when one connects the end points of the cuts which are inside the same index loop) which cut the diagram into disconnected pieces. In this subsection, I study the case in which a sequence of the cuts make up a loop, and this “cut-out loop” divides a diagram into two disconnected pieces, one of which does not contain the external legs (Fig.5). In this case, one can put the external momentum flow avoiding the region cut out by the cut-out loop. Without loss of generality, one can assume that there are no further cut-out loops inside¹⁷ the one under consideration. Then, since the type-1 and type-2 fields only mix through 1-2 or

¹⁶One does not need to worry about the case where n is a multiple of N in (3.2) in the strict $N \rightarrow \infty$ limit. Since the $N \rightarrow \infty$ limit is taken before the Fourier expansion. I thank S. Kalyana Rama and A. Sen for questions and comments on this point.

¹⁷For a loop on a sphere topology, inside and outside is a relative notion, but one may call one side inside and the other outside. Here I called the region of the Feynman diagram which does not contain the external legs as inside.

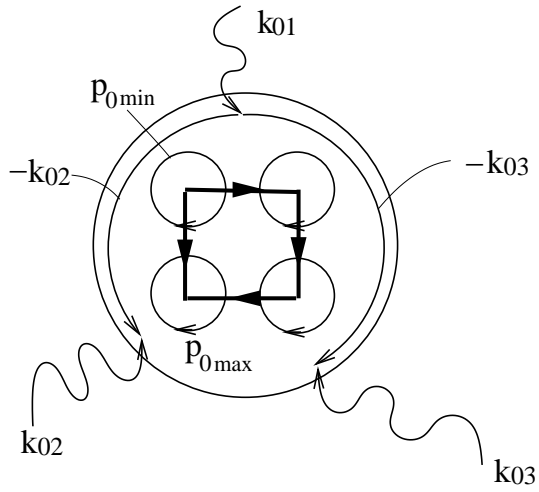


Figure 5: A diagram in which the sequence of the bold arrows surrounds a region without the external legs. The starting and the end points of the bold arrows are connected when they are inside of the same index loop. The bold arrows on the cuts are directed from the smaller to the larger momenta, following the rule given in Fig.7. In this case, there are a maximum and a minimum loop momenta among the momenta flowing through the cuts. The maximum momentum loop is the one where all the bold arrows come in, and the minimum momentum loop is the one where all those go out. Such diagrams vanish after the summation over the gauge index a_{max} or a_{min} .

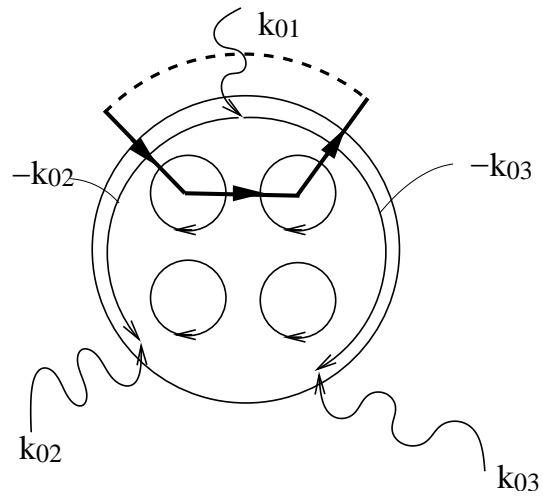


Figure 6: In this figure, the starting and the end points of the sequence of the bold arrows is connected, since they are inside of the same index loop (planar diagrams can be thought of as drawn on a sphere), as indicated by the dashed line. Thus the sequence of the bold arrows make up a cut-out loop. In non-vanishing diagrams, all cut-out loops divide the diagram into two disconnected pieces, both containing the external legs. In the above figure, the region containing the external leg with momentum k_{01} is separated from the region containing the external legs with momentum k_{02} and k_{03} by the cut-out loop.

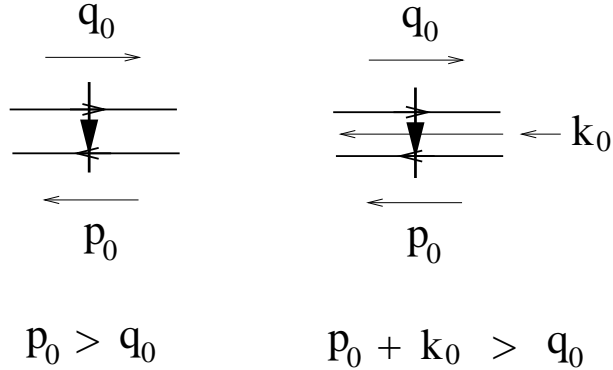


Figure 7: A bold arrow is put on the cut (temperature dependent part of the propagator, see Fig.4) to indicate which of the momenta associated with the index lines is larger. The direction is from the smaller to the larger momenta, and the sign of the loop momenta are determined referring to the direction of the associated index lines. When there is an external momentum flowing into a propagator (k_0 in the right), it is added to the momentum with the same direction. In other words, the direction of the bold arrow is determined according to the direction of the total momentum flowing on the propagator.

2-1 cut propagators, the cut out region consists of either entirely type-1 or entirely type-2 propagators and vertices. I first study the case in which the cut-out loop is either made of entirely 1-1 cuts or entirely 2-2 cuts. Other cases can be treated similarly. The correlation function is proportional to a product of the factors coming from the 1-1 or 2-2 cuts on this cut-out loop (see (2.36)):

$$\frac{1}{e^{|\beta(p_{0i}-p_{0j})+2\pi i \frac{a_i-a_j}{N}|_R} - 1} = \sum_{n=1}^{\infty} e^{-n|\beta(p_{0i}-p_{0j})+2\pi i \frac{a_i-a_j}{N}|_R}. \quad (3.3)$$

Contrary to the previous case, since $|\beta(p_{0i}-p_{0j})+2\pi i \frac{a_i-a_j}{N}|_R$ may have different signs for different combinations of (i, j) , the phases may cancel in the product. Then the summation over these gauge indices can have a non-zero value. However, there is always a maximum loop momentum, p_{0max} , and a minimum loop momentum, p_{0min} , among the loop momenta which cross the cuts on the cut-out loop. I denote the associated gauge indices a_{max} and a_{min} , respectively. Then, from the definition (2.37),

$$\left| \beta(p_{0max}-p_{0i}) + 2\pi i \frac{a_{max}-a_i}{N} \right|_R = \beta(p_{0max}-p_{0i}) + 2\pi i \frac{a_{max}-a_i}{N} \quad (3.4)$$

and

$$\left| \beta(p_{0\min} - p_{0i}) + 2\pi i \frac{a_{\min} - a_i}{N} \right|_R = - \left(\beta(p_{0\min} - p_{0i}) + 2\pi i \frac{a_{\min} - a_i}{N} \right), \quad (3.5)$$

i.e., they have a definite sign in any combination with other p_{0i} . (Recall that because of the on-shell delta function in (2.36), the difference between two momentum flows in a cut-propagator is always non-zero: $|p_{0i} - p_{0j}| = \omega$.) This means that in the Fourier expansion (3.3), the sign of the phase in $e^{2\pi i \frac{a_{\max}}{N}}$ *always* appears negative while that of $e^{2\pi i \frac{a_{\min}}{N}}$ *always* positive, and hence do not cancel. After summing over the index a_{\max} (or a_{\min}), the contribution from such diagrams vanish, as in (3.2). In Fig.5 the cut is drawn with a bold arrow which is directed from the smaller to the larger loop momenta, following the rule given in Fig.7. The maximum loop momentum $p_{0\max}$ (among the loop momenta which cross the cut-out loop) is the loop to which those bold arrows all come in, and the minimum $p_{0\min}$ is from which all those bold arrows flow out.

Essentially the same arguments hold for 1-2 (2-1) cuts. In this case, for $p_{0\max}$, for example, there is an extra overall factor $e^{\frac{1}{2}(\beta(p_{0\max} - p_{0i}) + 2\pi i \frac{a_{\max} - a_i}{N})}$ compared with the 1-1 or 2-2 cuts. Since type-1 and type-2 fields mix only through 1-2 or 2-1 cut propagators, and there are no further cuts inside the cut-out loop, the cut out region is made of either entirely type-1 fields or entirely type-2 fields. Then, an index line which enters from the type-1 region to the type-2 region must come out again.¹⁸ Therefore, there are always an even number of the extra phase factors coming from the 1-2 (2-1) cuts for each index loop, and they multiply up to integer powers of $e^{\beta p_{0\max} + 2\pi i \frac{a_{\max}}{N}}$. It partially cancels the relevant phase coming from the Fourier expansion of $1/(e^{(\beta(p_{0\max} - p_{0i}) + 2\pi i \frac{a_{\max} - a_i}{N})} - 1)$, but it does not completely cancel the phase factors. (This is basically because originally each of these was just half of the relevant phase).

3.3 The case in which every cut-out loop divides a diagram into two disconnected pieces both containing the external legs – some diagrams survive

From the discussions in the previous subsections, the non-vanishing contributions arise only from diagrams in which every cut-out loop divides the diagram into two disconnected

¹⁸Recall that every index loop has either zero or more than one cut in order for a diagram not to vanish.

pieces both containing the external legs (Fig.6). Here, the closed circuits made of cuts are interpreted as overlapping cut-out loops, as will be explained in more detail in the next subsection. In this case, the tree sub-diagram expressing the external momentum flow must cross the cut: Since the diagram is completely disconnected by the cut-out loop, there is no way to connect the separated external legs avoiding the cuts. For this kind of diagrams, the earlier argument does not hold, because an additional external momentum comes into the argument: Now it is possible to have $p_{0max} < p_{0i} + k_0$ or $p_{0min} + k_0 > p_{0i}$ for some i , where k_0 is an external momentum flowing into the cut propagator with index lines a_{max} and i , or a_{min} and i , respectively. From the definition (2.37), this means

$$\left| \beta(p_{0max} - (p_{0i} + k_0)) + 2\pi i \frac{a_{max} - a_i}{N} \right|_R = - \left(\beta(p_{0max} - (p_{0i} + k_0)) + 2\pi i \frac{a_{max} - a_i}{N} \right) \quad (3.6)$$

for some i , or

$$\left| \beta(p_{0min} + k_0 - p_{0i}) + 2\pi i \frac{a_{min} - a_i}{N} \right|_R = \beta(p_{0min} + k_0 - p_{0i}) + 2\pi i \frac{a_{min} - a_i}{N} \quad (3.7)$$

for some i . Compare these with the previous cases (3.4) and (3.5). Still, in order for a diagram not to vanish, there must not be an index loop where bold arrows are all coming in (as in the index loop associated with p_{0max} in the previous case), or all going out (as in that associated with p_{0min} in the previous case). In other words, when there is a bold arrow coming into an index loop, there must be at least one bold arrow which comes out of it. Thus the *directed* sequences of bold arrows make up closed circuits. Note that this can only happen when the sequence of the bold arrows crosses the external momentum flow, otherwise it is inconsistent with the definition of the bold arrows (i.e., the directed sequence of bold arrows should be along an increasing sequence of momenta, see Fig.7). In the next section, these non-vanishing diagrams will be studied in more detail.

4 Surviving diagrams as closed string tree diagrams in the real time formulation in the bulk

Now I will argue that the non-vanishing Feynman diagrams in the confined phase can be interpreted as tree diagrams of the real time formulation of closed string field theory on AdS at finite temperature.¹⁹ Here, the word “closed string theory” is used in a loose

¹⁹The reason I am using the phrase closed string *field* theory here is just to indicate that there will be propagators and interaction vertices for the type-2 *fields* in the bulk. The discussions remain within

sense, in that I regard random surfaces obtained from the Feynman diagrams of the large N gauge theories as closed string worldsheets [28], hoping more precise description as a closed string theory will emerge from the conjectured duality between closed string theories on AdS and large N gauge theories [2].²⁰

4.1 Cut-out loops as cuts of closed string propagators

First, I argue that the cut-out loops can be identified with the cuts of the temperature dependent parts of the closed string propagators. In closed string field theory, there is a freedom in separating the propagator and the interaction vertices (see e.g. [33]). However, it must be constructed in a way that it reproduces the correct perturbative diagrams. Therefore, in the following I do not specify how to divide the worldsheet into the propagators and interaction vertices, but the cut-out loop must be within the propagator part.

I will show that those cut-out loops give the correct energy dependence as the temperature dependent parts of closed string propagators in the real time formalism. I will discuss this in the free field limit, i.e. zero 't Hooft coupling limit. I expect that the discussions can be extended to finite 't Hooft coupling if the full propagators in the gauge theory instead of the free propagators are used.²¹

4.1.1 An isolated cut-out loop

I start with the case when the cut-out loop is isolated, i.e. all the index loops crossed by the cut-out loop have one incoming and one out going bold arrow. The case for more general closed circuits will be explained shortly. Notice first that the cut-out loop is proportional to $\delta(k_0^2 - (J\omega)^2)$, where k_0 is the momentum flowing into the cut-out loop and J is the number of the gauge theory propagators cut by the cut-out loop (Fig.8). This is due to the fact that on the cut-out loop, the bold arrows must be directed in the same direction, in order for the diagram not to vanish, as described in the previous section. This

perturbation theory. Non-perturbative studies using the field theory will be interesting but beyond the scope of this article.

²⁰See [29, 30, 31, 32, 8] for a recent attempt to describe precisely how the large N gauge theory correlation functions organize themselves into closed string amplitudes.

²¹I thank R. Gopakumar for reminding me that the following discussions on the energy dependence are for free field theory, and suggesting how the generalization to the finite 't Hooft coupling will be.

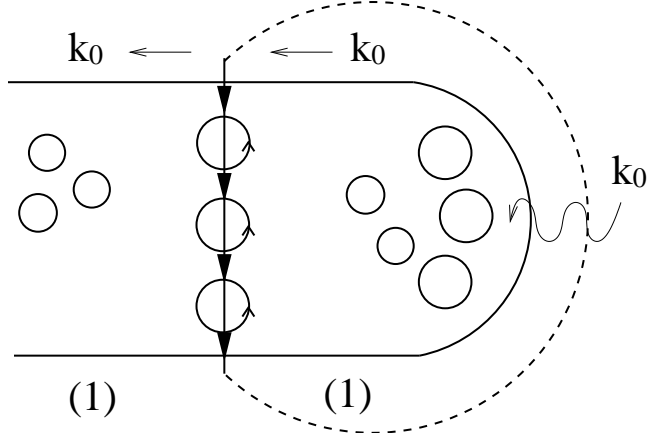


Figure 8: A 1-1 cut-out loop (the starting and the end points of the sequence of the bold arrows should be regarded as the same point, as indicated by the dashed line). The bold arrows are all in the same direction on the cut-out loop in order for the diagram not to vanish. The figure can be regarded as the case $k_0 = J\omega = 4\omega$, which is enforced by the on-shell delta functions of the cuts on the cut-out loop. “(1)” in the above refers to the type-1 region.

means that the momenta flowing through those cuts are either all ω or all $-\omega$. These give a factor $\delta(k_0 - J\omega)$ or $\delta(k_0 + J\omega)$, respectively. Up to these delta functions, both contributions are the same and one obtains $\delta(k_0^2 - (J\omega)^2)$. $J\omega$ corresponds to the external momentum flow on an edge of the tree sub-diagram which the cut-out loop crosses, and thus the cut-out loop can be assigned to a cut on an edge of the closed string tree diagram, i.e., a closed string propagator (Fig.9). In the free field limit, $J\omega$ can be identified with the energy of a closed string state corresponding to $\text{tr}\Phi^J$ [4, 34].²² Therefore, this is the correct on-shell delta function which should appear in the temperature dependent part of the propagators in the real time formalism: The temperature dependent part of the propagator in the real time formalism in general has a form of (2.36) without the gauge index dependent phase factors specific to the gauge theory in the confined phase. (Recall the derivation of (2.36) or see [16, 35].)

Furthermore, the 1-1 and 2-2 cut-out loops give rise to a following gauge index sum-

²²The concrete example in mind is $\mathcal{N} = 4$ super Yang-Mills theory compactified on S^3 , and ω is proportional to the inverse radius of the S^3 . Since this theory is conformal, after a suitable rescaling only the ratio of the two scales $\beta\omega$ is physically relevant.

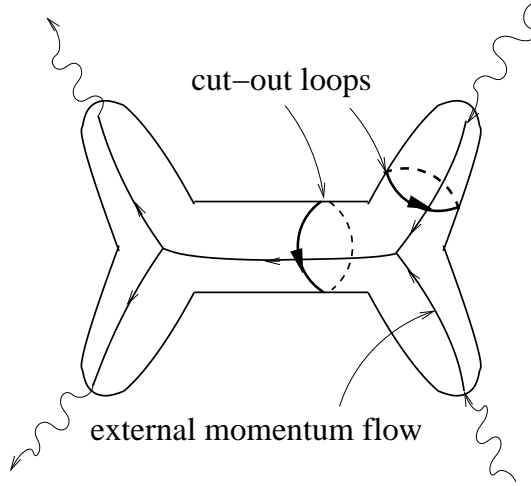


Figure 9: A ‘t Hooft Feynman diagram identified with a closed string worldsheet. The cut-out loop must cross the tree sub-diagram where the external momentum flows. Thus the cut-out loop can be identified with the cut on a closed string propagator.

mation:

$$\begin{aligned}
 \sum_{a_1=1}^N \cdots \sum_{a_J=1}^N \prod_{i=1}^J \frac{1}{e^{\beta\omega \pm 2\pi i \frac{a_i-a_{i+1}}{N}} - 1} &= \sum_{a_1=1}^N \cdots \sum_{a_J=1}^N \prod_{i=1}^J \sum_{n_i=1}^{\infty} e^{-n_i(\beta\omega \pm 2\pi i \frac{a_i-a_{i+1}}{N})} \\
 &= \sum_{n=1}^{\infty} e^{-n\beta\omega J} \\
 &= \frac{1}{e^{\beta\omega J} - 1}.
 \end{aligned} \tag{4.1}$$

Here, $a_{J+1} = a_1$. Recall that the total momentum of the cuts on the cut-out loop are either all ω or all $-\omega$, and \pm respectively correspond to each case: The contribution from $\delta(p_{0i} - p_{0j} + k_0) \mp \omega$, where p_{0i} and p_{0j} are loop momenta associated with the index a_i and a_j , and k_0 is a possible external momentum flow (on one of the cuts). Notice that from the first line to the second line, the sum over the gauge indices only picked up the $n_1 = n_2 = \cdots = n_J \equiv n$ contributions, since the phases must cancel to give a non-zero result. Similarly, the 1-2 and 2-1 cut-out loops give rise to a factor

$$\begin{aligned}
 \sum_{a_1=1}^N \cdots \sum_{a_J=1}^N \prod_{i=1}^J \frac{e^{\frac{1}{2}(\beta\omega + 2\pi i \frac{a_i-a_{i+1}}{N})}}{e^{\beta\omega \pm 2\pi i \frac{a_i-a_{i+1}}{N}} - 1} &= e^{\frac{\beta}{2}\omega J} \sum_{a_1=1}^N \cdots \sum_{a_J=1}^N \prod_{i=1}^J \sum_{n_i=1}^{\infty} e^{-n_i(\beta\omega \pm 2\pi i \frac{a_i-a_{i+1}}{N})} \\
 &= e^{\frac{\beta}{2}\omega J} \sum_{n=1}^{\infty} e^{-n\beta\omega J}
 \end{aligned}$$

$$= \frac{e^{\frac{\beta}{2}\omega J}}{e^{\beta\omega J} - 1}. \quad (4.2)$$

Again, the factors (4.1) and (4.2) are the expected ones for the temperature dependent parts of the propagators in the real time formalism. All together, these give the correct energy dependent factors to be interpreted as the temperature dependent part of the propagators in the real time formulation of closed string field theory at finite temperature.

4.1.2 Closed circuits as overlapping cut-out loops

So far, I have studied the case in which cut-out loops are isolated. In general, bold arrows make up closed circuits: More than two bold arrows can come in and go out at one index-momentum loop (Fig.10) to give a non-vanishing contribution. This case can be treated as an overlap of single cut-out loops. To see this, it may be useful to draw an analogy between the bold arrow circuits with Feynman diagrams:²³ The bold arrows can be put on the edges of the dual graph of a 't Hooft-Feynman diagram. The dual graph can be obtained by replacing the faces of the original graph by dual vertices, the edges by orthogonal dual edges and the vertices by dual faces (Fig.10). The bold arrows make up closed circuits on the dual graph of the planar Feynman diagram. When one Fourier expands the correlation function in terms of the gauge index dependent factor $e^{-2\pi i \frac{a_i}{N}}$, the bold arrow tells whether the phase $2\pi i \frac{a_i}{N}$ from the propagator which it crosses appears with positive sign or negative sign. In the limit $N \rightarrow \infty$, $\frac{a_i}{N} \rightarrow \theta_i$, which was implicit in the above, one can regard the Fourier mode as an analogue of discrete "momentum". Then, each index sum picks up a term in which all of the phases cancel. This is an analogue of the momentum conservation at each vertex on Feynman diagrams. One can solve the "momentum conservations" to end up with "loop momenta" for sub-loops of the circuit, see Fig.11-13. Note that I have specified the direction of the bold arrows, so the "momentum" should be always positive, i.e. either positive incoming or positive outgoing. The circuits with the same topology but with different directions of arrows should be regarded as different circuits. Each sub-loop on the cut-out circuit has a direction inherited from the direction of the bold arrows of the cut-out circuit, in particular must cross an edge of the tree sub-diagram which expresses the external momentum flow, as in the case of the single cut-out loop. Thus as before it can be associated with an edge of a closed string tree diagram. The

²³The analogy here is with general Feynman diagrams, not with the specific large N Feynman diagrams which have been studied in this article.

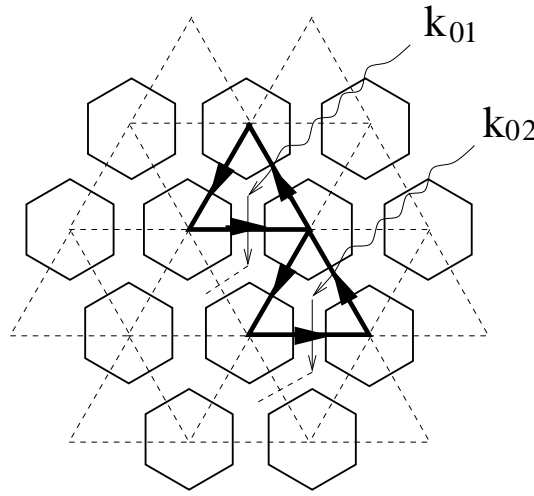


Figure 10: A part of a planar 't Hooft-Feynman diagram (the double lines) and its dual graph (the dashed lines). The cut-out lines (bold arrows) make up a closed circuit on the dual graph. Each sub-loop of the closed circuits must surround a region with the external leg, and there must be at least one external leg on the other side, as described in section 3.3.

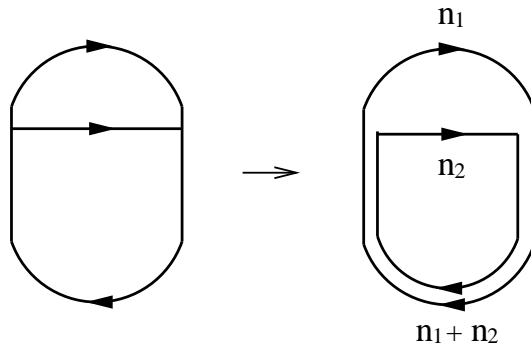


Figure 11: A closed circuit with the “momentum conservation” at each vertex. The “momentum conservations” can be solved by assigning “loop momenta” to the sub-loops in the circuit.

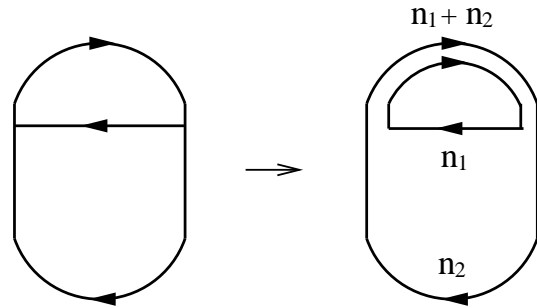


Figure 12:

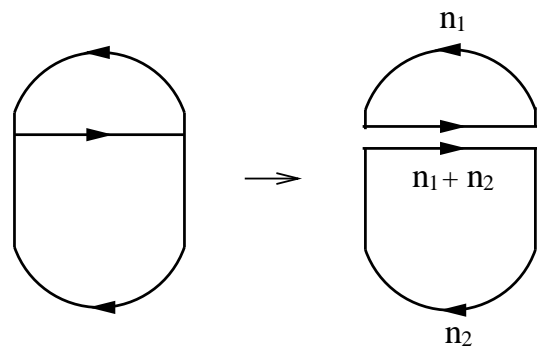


Figure 13:

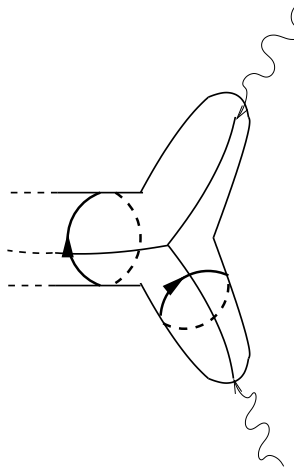


Figure 14: An example of a closed string tree diagram in which the circuit of the type Fig.11 appears. If one draws a corresponding gauge theory Feynman diagram on a plane (view the above worldsheet from the right), the cut-out loops look as depicted in the righthand side of Fig.11. The closed circuit in the lefthand side of Fig.11 can be interpreted as a limit where two cut-out loops (partially) overlap.

energy dependent factor of each sub-loop is the same as that of a single cut-out loop. Therefore, one can interpret such a sub-loop as a single cut-out loop: Closed circuits are interpreted as made of overlapping cut-out loops (Fig.14-16).

As an example, below I study the case where two cut-out loops overlap at one index loop (Fig.10), again in the free limit. The external momenta entering into cut-out loops are k_{01} and k_{02} . I assume that both of the cut-out loops are 1-1 cut out loops, other cases can be treated similarly. These two cut-out loops give a contribution proportional to the factor

$$\begin{aligned}
& \sum_{a_1=1}^N \cdots \sum_{a_J=1}^N \sum_{b_1=1}^N \cdots \sum_{b_J=1}^N \prod_{i=1}^{J_1} \prod_{j=1}^{J_2} \delta_{a_1 b_1} \frac{1}{e^{\beta\omega+2\pi i \frac{a_i-a_{i+1}}{N}} - 1} \cdot \frac{1}{e^{\beta\omega+2\pi i \frac{b_j-b_{j+1}}{N}} - 1} \\
&= \sum_{a_1=1}^N \cdots \sum_{a_J=1}^N \sum_{b_1=1}^N \cdots \sum_{b_J=1}^N \prod_{i=1}^{J_1} \prod_{j=1}^{J_2} \delta_{a_1 b_1} \sum_{n_i=1}^{\infty} \sum_{m_j=1}^{\infty} e^{-n_i(\beta\omega+2\pi i \frac{a_i-a_{i+1}}{N})} e^{-m_j(\beta\omega+2\pi i \frac{b_j-b_{j+1}}{N})} \\
&= \sum_{n=1}^{\infty} e^{-n\beta\omega J_1} \cdot \sum_{m=1}^{\infty} e^{-m\beta\omega J_2} \\
&= \frac{1}{e^{\beta\omega J_1} - 1} \cdot \frac{1}{e^{\beta\omega J_2} - 1}.
\end{aligned} \tag{4.3}$$

Here, J_1 and J_2 are the numbers of the bold arrows on the cut-out loops and $a_1 = b_1$

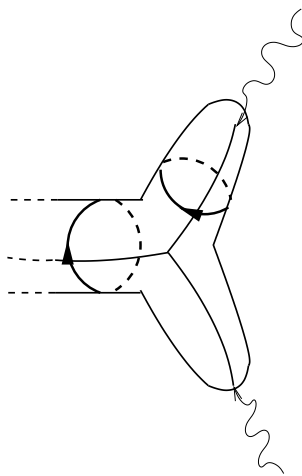


Figure 15: An example of a closed string tree diagram in which the circuit of the type Fig.12 appears.

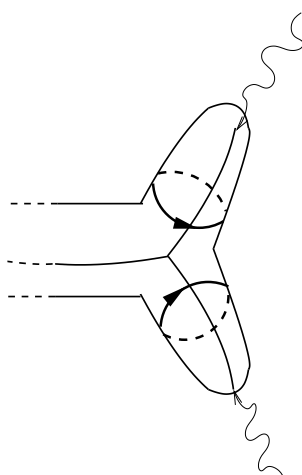


Figure 16: An example of a closed string tree diagram in which the circuit of the type Fig.13 appears.

is the index of the index loop where two cut-out loops overlap. From the second line to the third line of (4.3), the “momentum conservation” was explicitly solved by using the “loop momenta” n and m . Eq.(4.3) is the correct factor for the contributions from two cuts in the real time formulation of closed string field theory at finite temperature. One can also obtain the on-shell delta functions $\delta(k_{01}^2 - (J_1\omega)^2)$ and $\delta(k_{02}^2 - (J_2\omega)^2)$, as in the case of a single cut-out loop.

4.2 Closed string interaction vertices

Next, I argue that the interaction vertices for the closed string field theory arising from the gauge theory Feynman diagrams also have the desired property as required by the real time formalism. Recall that each cut out region are either made of entirely type-1 or entirely type-2 propagators and vertices. Also recall that the 2-2 propagator is the complex conjugate of the 1-1 propagator (see (2.35)):

$$iD_0^{(22)}(k_0) = (iD_0^{(11)}(k_0))^*. \quad (4.4)$$

Similarly, for the type-1 and type-2 interaction vertices (2.38):

$$i \text{tr}V_2[\Phi_{(2)}] = (i \text{tr}V_1[\Phi_{(1)}])^* \Big|_{\Phi_{(1)} \rightarrow \Phi_{(2)}}. \quad (4.5)$$

For a given diagram with a cut-out type-2 region, there is a corresponding diagram which is obtained by replacing all the type-2 propagators and vertices in the region by those of type-1 (Fig.17,18). Then, the contribution of the type-2 region is the complex conjugate of the corresponding type-1 region. This means that the type-2 vertices of the closed string field theory obtained from the gauge theory are the complex conjugate of the corresponding type-1 vertices. This is the property of the interaction vertices in the real time formulation of finite temperature field theories.

Finally, recall that in each cut-out region there are no further cuts, i.e. no further temperature dependent piece. This means that these cut-out regions probe the zero-temperature geometry of the bulk, i.e. AdS_5 for the four dimensional $\mathcal{N} = 4$ super Yang-Mills theory on S^3 .²⁴

²⁴Since I have been studying a quantum mechanics dimensionally reduced from four dimensions, strictly speaking I have only considered the s-wave for the S^3 part of the coordinates on AdS_5 . But generalization to include excited modes on the S^3 will be straightforward.

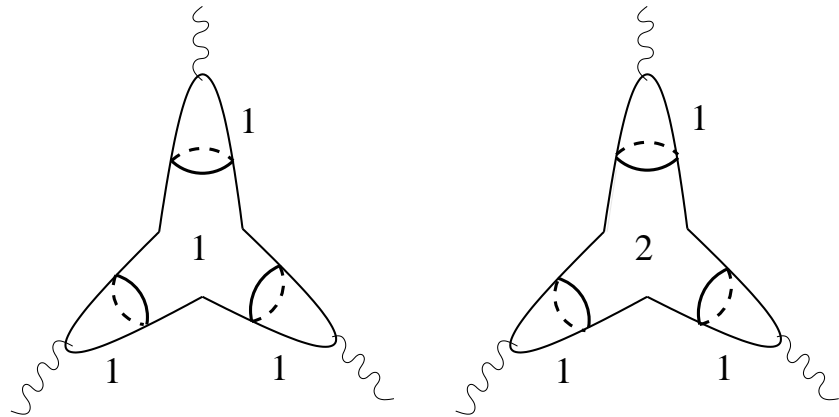


Figure 17: Feynman diagrams divided into type-1 regions and type-2 regions by the cut-out loops. The type-2 region in the diagram on the right is complex conjugate to the corresponding type-1 region in the diagram on the left.

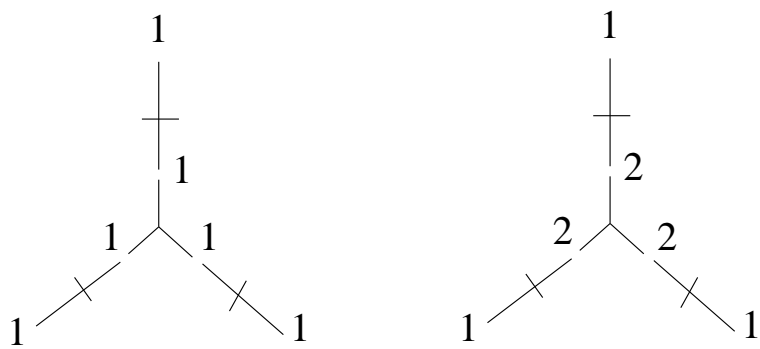


Figure 18: The diagrams in Fig.17 drawn so that they look as diagrams in the real time formulation of finite temperature field theories.

Thus altogether, the real time formulation of the gauge theory at finite temperature in the confined phase describes the real time formulation of classical closed string field theory on AdS at finite temperature.

5 Summary and Discussions

Summary

Successful tests of the AdS-CFT conjecture encourage our hope that it has the answers to all the puzzles surrounding black holes, at least in asymptotically AdS spaces. However, to extract such answers, one needs to understand how to translate closed string descriptions to gauge theory descriptions and vice versa, in particular what distinguishes between the geometries with and without a black hole in the gauge theory descriptions. And to solve real puzzles about black holes, one must work with the Lorentzian signature.

In this article, I have given a prescription for extracting the dual bulk description corresponding to the confined phase in the real time formulation of gauge theories at finite temperature. With this prescription, I have shown how the difference between the phases, namely the confined and the deconfined phases, changes the relevant Feynman diagrams in the planar limit. In the confined phase, the Feynman diagrams of the gauge theory organize themselves into tree diagrams of closed string field theory on AdS at finite temperature in the real time formalism.

Study from the closed string side

In this article, I have compared the gauge theory results with the quite general properties of the real time formulation of the closed string field theory. It is certainly interesting to re-examine the real time formulation of closed string field theory at finite temperature [35] in more detail, in comparison with the analysis of the large N Feynman diagrams in this article.²⁵ Since what one directly obtains from the 't Hooft-Feynman diagrams are closed string worldsheets rather than the string field theory, it may also be useful to investigate the worldsheet formulation of the real time formalism [38]. In particular, it will be nice if

²⁵In the BMN plane wave limit [36], the real time formulation of light-cone string field theory was recently studied in [37]. However, note that the BMN limit is a different limit from the 't Hooft limit.

one can characterize the cut-out loop in terms of the closed string worldsheet language, and see the parallel between the results in this article.²⁶

Deconfinement, Hawking-Page and the Kosterlitz-Thouless transition

In the deconfined phase, a different type of Feynman diagram, namely a diagram with unrestricted cuts, becomes relevant. This difference should be reflecting the distinction between the geometry with and without a black hole, as long as the identification of confinement-deconfinement phase transition with the Hawking-Page transition is correct. This may be regarded as a Lorentzian signature counterpart of the Kosterlitz-Thouless phase transition on the string worldsheet [40, 41, 42]. There the condensation of the winding modes makes the string worldsheet interpretation difficult. The mechanism that is supposed to be corresponding to the Kosterlitz-Thouless phase transition in the large N Feynman diagrams was discussed in [8] (see also [43]). It has long been anticipated that the Kosterlitz-Thouless phase transition on the string worldsheet is analogous to the deconfinement phase transition where underlying degrees of freedom manifests itself. It is intriguing that in the AdS-CFT correspondence this is not just an analogue but exactly the same thing (the equivalent dual description). The endpoint of the phase transition may still admit a worldsheet interpretation in a *different* geometry [8, 44, 45, 46, 47], however, this point needs further study.²⁷ Note that the Euclidean case studied in the references mentioned above is somewhat simplified situation compared with the original Lorentzian problem, since the former only contains the region outside the black hole horizon.

The role of the imaginary time formalism

The prescription I have given for reading off the dual description of the confined phase uses the Matsubara contour to determine the boundary conditions for the thermal Green's function. In this sense, the real time formalism is not completely different from the

²⁶In the case of a worldsheet with a torus topology, the cut-out loop (in my terminology) was characterized by a boundary condition [39].

²⁷Historically, string theory started as a description of confinement. From this point of view, the correspondence between the deconfined phase and the black hole geometry makes it highly non-trivial if the black hole geometry still allows a string description. It might be the case that such a description is possible only for a specific class of observers (coordinate frames), as suggested by the black hole complementarity [48].

imaginary time formalism but rather it contains the latter in the imaginary direction of the contour. The relevance of the Matsubara contour for determining the boundary condition reminds us of the role of the Euclidean path integral in the models of gravitational physics [49, 7, 50] (see also [1]).

In the gauge theory context, the relevance of the Matsubara contour indicates that the methods which are useful in the imaginary time formalism may have direct relevance also in the real time formalism. In particular, the crucial role played by the temporal component of the gauge field in this article seems to suggest that the Polyakov's criterion for confinement [51] has some simple extension to the real time formalism. Note that the boundary condition is not just a simple consequence of the projection onto the gauge singlet sector, but also includes the saddle point calculation. It is important to further investigate this role of the imaginary time formalism in the real time formalism.

On dynamical formation of black holes

How a black hole is formed from ordinary matter is an important question, which is also relevant for the information loss paradox [52]. I would like to point out that to describe such a process, the initial geometry without the black hole should be probed by the prescription I have given, namely by taking into account the configuration of the temporal component A_0 of the gauge field, characteristic of the confined phase, on the vertical parts of the contour. Moreover the final state, the large black hole in AdS space,²⁸ should correspond to the gauge theory in the deconfined phase.

Formation of a black hole is a dynamical process, and it may be worth mentioning that the real time formalism has a close relation with the Schwinger-Keldish technique for describing non-equilibrium systems [53, 54]. The techniques developed in this article may also find application in the study of non-equilibrium processes in large N gauge theories. It will be interesting to apply the Schwinger-Keldish technique to the large N gauge theories to study the dynamical formation of a black hole via the AdS-CFT correspondence.

²⁸Large here means the larger of the two Schwarzschild-AdS solutions in [3].

Statistical average and horizon

In this article I have argued that the real time formulation of gauge theories at finite temperature can describe the dual closed string field theory on AdS at finite temperature. Together with the results in the black hole phase [1], the success in describing *both* the black hole and the non-black hole phase by the real time formulation of gauge theory at finite temperature is an encouraging evidence for the AdS-CFT correspondence in Lorentzian signature. On the other hand, the real time formulation introduces the doubled degrees of freedom to describe the thermal ensemble by entanglement.²⁹ The reason one usually uses a statistical average is that one does not need to know the state one is precisely in, to describe the thermodynamical property of the system. However, one expects that there is actually a single pure state at a given moment, and unitarity may be understood more straightforwardly without taking the statistical ensemble, even though the real time formulation of field theory at finite temperature is unitary. It should be interesting to understand more precisely what actually the statistical average in the gauge theory side introduces in the bulk geometry. This question may be related to the recent proposal of [55]. See also [1].

$1/N$ effects

In this article I worked in the leading order in the $1/N$ expansion. This corresponds to the classical closed string theory in the bulk. This was sufficient since the argument from the Carter-Penrose diagram is based on classical gravity. However, it is also important to study how the $1/N$ corrections, which corresponds to quantum corrections in the bulk, modify the above classical view.³⁰ Also, the information paradox arose from the discovery of Hawking radiation [57] which is a quantum effect. The method developed in [9] may be useful for the investigation in this direction.

²⁹This statement may be more appropriate for the thermo field dynamics. The Feynman rules derived from the thermo field dynamics are the same [13] as those of the real time formulation of Ref.[14].

³⁰The role of the $1/N$ corrections in a related context was stressed in [56]. The sum over contributions from both the AdS-Schwarzshild black hole geometry and the AdS geometry discussed in [1] is a non-perturbative effect in $1/N$. Note that even though the contributions must be summed over, each saddle point in the gauge theory should have a dual bulk interpretation, at least at large N . The objective of this article has been to read off, or ultimately *derive*, the bulk geometry from the gauge theory.

More puzzles than have been solved?

In the confined phase, the two-point Green's function between a type-1 and a type-2 operator should be identified with 1-2 propagator in closed string field theory. This is quite natural as a dual description of the confined phase still at finite temperature. In contrast, despite some successes in the comparisons between gauge theories in deconfined phase and black hole geometry in literature, it is still not clear precisely *how* correlation functions in the large N gauge theory describe the dual theory on the black hole geometry. This raises a question as to how the dual of deconfined phase is encoded in the gauge theory correlation functions. In the spirit followed in this article for the confined phase, one should also be able to describe from the gauge theory how the type-2 fields are organized in the deconfined phase into the degrees of freedom behind the horizon. Thus the answer to the question raised in the introduction: “How does confinement change the role of type-2 fields in the bulk?” now comes back as a question to the original interpretation: *Precisely how does deconfinement change the role of the type-2 fields in the bulk?*³¹

Acknowledgments

It is my pleasure to express my thanks to D. Astefanesei, J. R. David, D. Ghoshal, R. Gopakumar, D. P. Jatkar, S. Naik, A. Sen, K. Sengupta and K. P. Yogendran for useful discussions and valuable comments which substantially improved the quality of this article. I am also grateful to D. Ghoshal, N. Mahajan and K. P. Yogendran for careful reading of the manuscript and various useful suggestions. I sincerely appreciate liberal support for our research from the people in India.

Appendix

A A sample calculation

In this appendix, I provide a simple example to illustrate how the mechanism which selects the surviving Feynman diagrams in the confined phase works. I calculate the two-point function $\langle \text{tr}\Phi_{(1)}^2(k_0)\text{tr}\Phi_{(1)}^2(-k_0) \rangle$ (the total momentum conservation delta function has

³¹I thank J. R. David for raising this question.

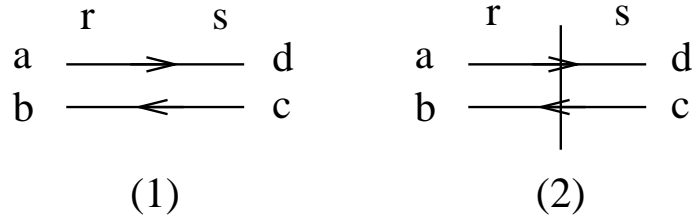


Figure 19: Feynman propagators. a, c refer to the first gauge index of the adjoint field $\Phi_{(r)ab}$, and b, d refer to the second. $r, s = 1, 2$ refer to type-1 and type-2.

been dropped), where $\Phi_{(1)}$ is the type-1 adjoint scalar field, in the free limit of the $SU(N)$ gauge quantum mechanics. The case for the correlation functions with type-2 fields are similar. The calculation follows the explanation in the main text, and should be compared with the general arguments there. This simple example still captures the essential points of the mechanism which selects the non-vanishing diagrams in the confined phase. In the following, all the overall constants are omitted since they are not important for the present purpose. Since I am studying the free theory in this example, I only need to recall the propagators (2.35) and (2.36). These are depicted in Fig.19. The first corresponds to the temperature independent part

$$iD_{0ab,cd} = \delta_{ad}\delta_{bc} \begin{pmatrix} \frac{i}{k_0^2 - \omega^2 + i\epsilon} & 0 \\ 0 & \frac{-i}{k_0^2 - \omega^2 - i\epsilon} \end{pmatrix}. \quad (\text{A.1})$$

The matrix structure of the propagator originates from the fact that one needs to include two types of fields, type-1 and type-2, for describing the real time formulation of the finite temperature field theory. The (1-1) matrix component corresponds to the type-1-type-1 propagator, and so on. The second in Fig.19 corresponds to the temperature dependent part of the propagator

$$\begin{aligned} iD_{\beta ab,cd} &= \delta_{ad}\delta_{bc}\pi\delta(k_0^2 - \omega^2) \\ &\quad \frac{1}{e^{|\beta k_0 + 2\pi i \frac{a-b}{N}|_R} - 1} \begin{pmatrix} 1 & e^{\frac{1}{2}|\beta k_0 + 2\pi i \frac{a-b}{N}|_R} \\ e^{\frac{1}{2}|\beta k_0 + 2\pi i \frac{a-b}{N}|_R} & 1 \end{pmatrix}. \end{aligned} \quad (\text{A.2})$$

The temperature dependent part of the propagator is drawn with the “cut”, i.e. the vertical line in the Fig.19 (2). This cut is one of the main tools in the following discussions. The relevant Feynman diagrams are depicted in Fig.20-22. The total momentum flowing on a propagator is a sum of momenta on its two index lines (taking into account the

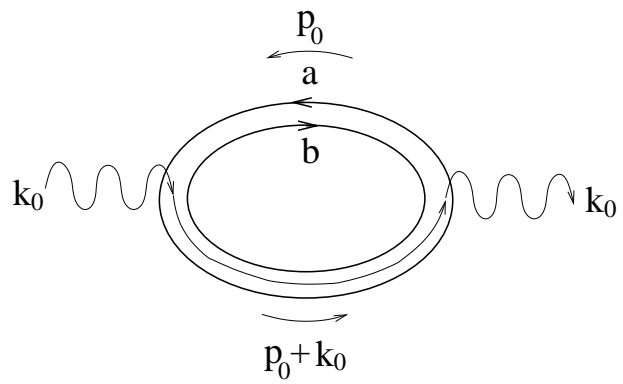


Figure 20: A Feynman diagram with no cut contributing to $\langle \text{tr} \Phi_{(1)}^2(k_0) \text{tr} \Phi_{(1)}^2(-k_0) \rangle$.

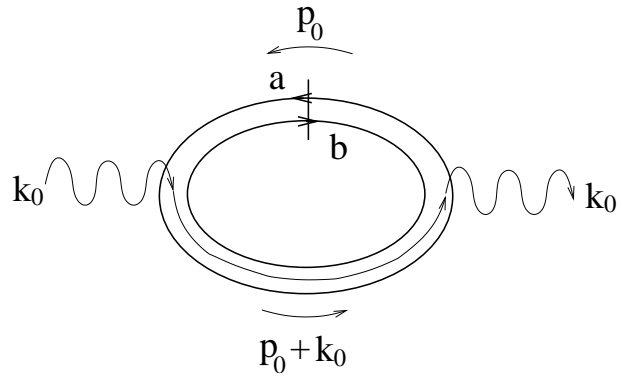


Figure 21: The one-cut contribution to $\langle \text{tr} \Phi_{(1)}^2(k_0) \text{tr} \Phi_{(1)}^2(-k_0) \rangle$.

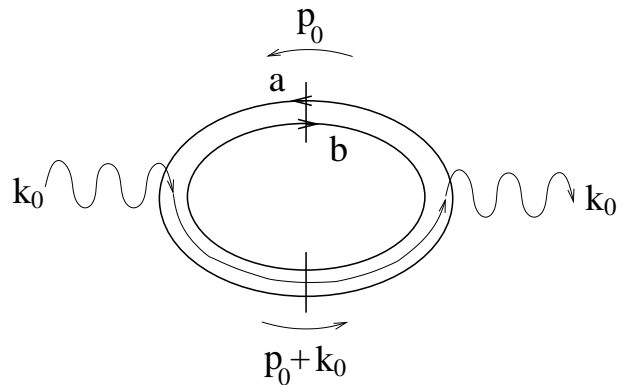


Figure 22: The two-cut (cut-out) contribution to $\langle \text{tr} \Phi_{(1)}^2(k_0) \text{tr} \Phi_{(1)}^2(-k_0) \rangle$.

signs indicated by the arrows), and external momentum (k_0 in this case) flowing between the double lines if there is any. Fig.20 is the temperature independent contribution and probes the zero-temperature bulk geometry. The calculation is standard so I omit the explanation of this case, see e.g. [29, 30, 31, 32, 8].³²

A.1 Only one cut on an index loop

Fig.21 has one cut, that is, the temperature dependent part. In this case, one can parameterize the loop integration variable p_0 so that the external momentum flows through the propagator without the cut, as shown in Fig.21. This Feynman diagram gives

$$\sum_{a=1}^N \sum_{b=1}^N \int dp_0 \frac{i}{p_0^2 - \omega^2 + i\epsilon} \delta((p_0 + k_0)^2 - \omega^2) \frac{1}{e^{|\beta(p_0 + k_0) + 2\pi i \frac{a-b}{N}|_R} - 1}. \quad (\text{A.3})$$

In a planar diagram, one can associate each loop momentum to an index loop: The number of the index loop is one more than the number of the loop momentum, but one index sum can be factored out. Here, the sum over the index b can be factored out by the shift $a \rightarrow a+b \pmod{N}$. The rest of the indices are “associated” to the loop momentum, in this case a to p_0 : The gauge index and the loop momentum appear in a specific combination $\beta p_0 + 2\pi i \frac{a}{N}$. After performing the p_0 integration using the delta function, one obtains (the overall factor N coming from the sum over the index b has been dropped)

$$\begin{aligned} & \frac{1}{2\omega} \sum_{a=1}^N \frac{i}{(\omega - k_0)^2 - \omega^2 + i\epsilon} \frac{1}{e^{|\beta\omega + 2\pi i \frac{a}{N}|_R} - 1} \\ & + \frac{1}{2\omega} \sum_{a=1}^N \frac{i}{(\omega + k_0)^2 - \omega^2 + i\epsilon} \frac{1}{e^{|\beta\omega + 2\pi i \frac{a}{N}|_R} - 1}. \end{aligned} \quad (\text{A.4})$$

The first term in (A.4) contains a factor

$$\sum_{a=1}^N \frac{1}{e^{|\beta\omega + 2\pi i \frac{a}{N}|_R} - 1} = \sum_{a=1}^N \sum_{n=1}^{\infty} e^{-n|\beta\omega + 2\pi i \frac{a}{N}|_R} = 0 \quad (\text{A.5})$$

and vanishes. Recall that $|\dots|_R$ was defined in (2.37) as

$$|z|_R = \begin{cases} z & (\text{Re } z > 0) \\ -z & (\text{Re } z < 0) \end{cases}, \quad (\text{Re } z \neq 0). \quad (\text{A.6})$$

More precisely, I took N to be strictly infinite so that the sum $\sum_{a=1}^N$ can be replaced with the integral $N \int_0^1 d\theta$. This picks out the constant mode in the Fourier expansion on the

³²And see [58] for a prescription for the Lorentzian signature.

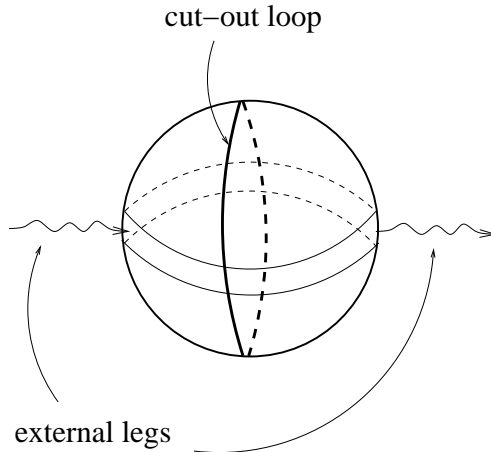


Figure 23: The Feynman diagram in Fig.22 drawn on a sphere. The end points of the cuts are connected if they are inside the same index loop, to make up a cut-out loop. The cut-out loop divide the sphere into two regions both containing an external leg.

left hand side of (A.5), which is zero. As explained in the main text, (A.5) is the basic equation which is relevant for the vanishing of a large class of Feynman diagrams in the confined phase. The second term in (A.4) also vanishes in the same way.

A.2 The case in which a cut-out loop divides the diagram into two pieces both containing an external leg

Now let us turn to the calculation of Fig.22. In Fig.22, the two cuts divide the diagrams to two disconnected pieces both containing an external leg. If one connects the end points of the cuts inside the same index loop, the cuts make up a cut-out loop (Fig.23). The point is that in this case, the external momentum flow must cross the cut, in contrast to the previous case. Since two regions of the diagram are disconnected by the cuts, one cannot avoid the cut by a shift of loop integration variable p_0 . The Feynman diagram is calculated to be

$$\sum_{a=1}^N \sum_{b=1}^N \int dp_0 \delta(p_0^2 - \omega^2) \frac{1}{e^{|\beta p_0 + 2\pi i \frac{a-b}{N}|_R} - 1} \delta((p_0 + k_0)^2 - \omega^2) \frac{1}{e^{|\beta(p_0 + k_0) + 2\pi i \frac{a-b}{N}|_R} - 1}. \quad (\text{A.7})$$

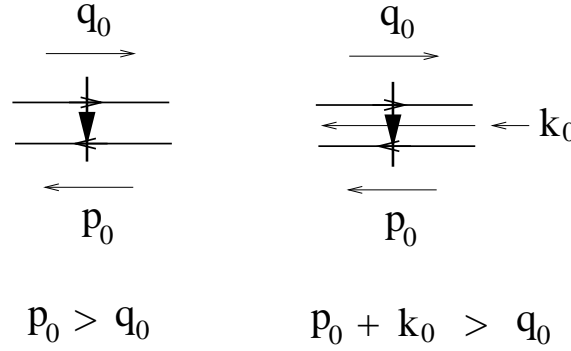


Figure 24: A bold arrow put on a cut indicates which of the momenta associated with the index is larger. When there is an external momentum flowing into a propagator (k_0 in the right), it is added to the momentum with the same direction.

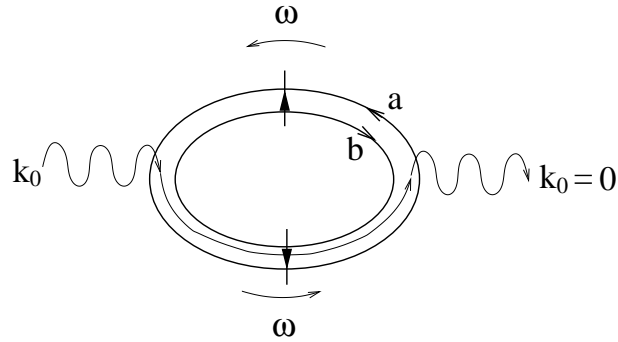


Figure 25: The vanishing cut-out diagram.

As in the previous case, one summation over gauge indices factors out. After performing the loop integral one obtains

$$\sum_{a=1}^N \frac{1}{e^{|\beta\omega+2\pi i \frac{a}{N}|_R} - 1} \delta((\omega + k_0)^2 - \omega^2) \frac{1}{e^{|\beta(\omega+k_0)+2\pi i \frac{a}{N}|_R} - 1} \quad (\text{A.8})$$

$$+ \sum_{a=1}^N \frac{1}{e^{|\beta\omega+2\pi i \frac{a}{N}|_R} - 1} \delta((-\omega + k_0)^2 - \omega^2) \frac{1}{e^{|\beta(-\omega+k_0)+2\pi i \frac{a}{N}|_R} - 1}. \quad (\text{A.9})$$

A.2.1 The vanishing case

The first line (A.8), a contribution from $p_0 = \omega$ case, can be divided into two cases: $k_0 = 0$ and $k_0 = -2\omega$. Fig.25 corresponds to the $k_0 = 0$ case. Following the rule given in Fig.24, I put bold arrows on the cuts to indicate which of the directed momenta is larger. The

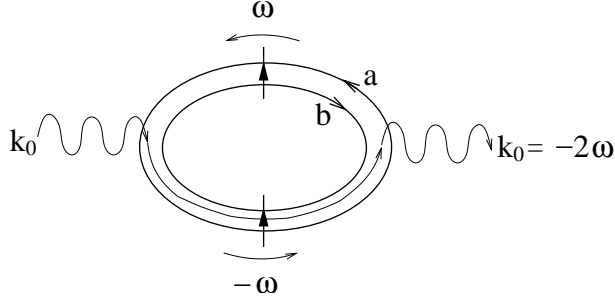


Figure 26: The non-vanishing cut-out diagram.

external momentum flow is added to the loop momentum in the same direction. In other words, the direction of the bold arrow is determined according to the direction of the total momentum flowing on a propagator. The momentum associated with the factored out index is regarded as zero. In Fig.25, the bold arrows are always directed from the b -index line to a -index line. This means that the momenta on the a -index line is always bigger than that of the b -index line (which is regarded as zero, as mentioned above). Therefore, Fig.25 is a contribution to Fig.22 in the following situation:

$$\left| \beta p_0 + 2\pi i \frac{a}{N} \right|_R = \beta p_0 + 2\pi i \frac{a}{N} \quad (\text{A.10})$$

$$\left| \beta(p_0 + k_0) + 2\pi i \frac{a}{N} \right|_R = \beta(p_0 + k_0) + 2\pi i \frac{a}{N}, \quad (\text{A.11})$$

where $|\cdots|_R$ was defined in (A.6). Thus I obtain

$$\begin{aligned} & \frac{1}{2\omega} \sum_{a=1}^N \frac{1}{e^{|\beta\omega+2\pi i \frac{a}{N}|_R} - 1} \delta(k_0) \frac{1}{e^{|\beta\omega+2\pi i \frac{a}{N}|_R} - 1} \\ &= \frac{1}{2\omega} \delta(k_0) \sum_{a=1}^N \sum_{n_1=1}^{\infty} e^{-n_1(\beta\omega+2\pi i \frac{a}{N})} \sum_{n_2=1}^{\infty} e^{-n_2(\beta\omega+2\pi i \frac{a}{N})} = 0. \end{aligned} \quad (\text{A.12})$$

The point is that the sign of the phase $2\pi i \frac{a}{N}$ in the Fourier expansion is always the same. This is a consequence of (A.10) and (A.11), which are indicated by the bold arrows in Fig.25. There are no cancellations of the a -dependent phases and hence it vanishes upon summation over gauge index a , like in the previous case (A.5).

A.2.2 The non-vanishing case

Now let us turn to the $k_0 = -2\omega$ case in (A.8). This corresponds to Fig.26. In this case, in the upper propagator the bold arrow is directed from the b -index line to a -index

line, whereas in the lower propagator the direction is reversed. This means that the momentum in the direction of a -index line is bigger than that in the direction of the b -index line in the upper propagator, and smaller in the lower one (Fig.24). Therefore, Fig.26 is a contribution to Fig.22 in the following situation:

$$\left| \beta p_0 + 2\pi i \frac{a}{N} \right|_R = \beta p_0 + 2\pi i \frac{a}{N} \quad (\text{A.13})$$

$$\left| \beta(p_0 + k_0) + 2\pi i \frac{a}{N} \right|_R = - \left(\beta(p_0 + k_0) + 2\pi i \frac{a}{N} \right). \quad (\text{A.14})$$

Notice the difference from the previous case, (A.10) and (A.11). Then, (A.8) results in a non-zero factor

$$\begin{aligned} & \frac{1}{2\omega} \sum_{a=1}^N \frac{1}{e^{|\beta\omega+2\pi i \frac{a}{N}|_R} - 1} \delta(k_0 + 2\omega) \frac{1}{e^{|\beta\omega+2\pi i \frac{a}{N}|_R} - 1} \\ &= \frac{1}{2\omega} \delta(k_0 + 2\omega) \sum_{a=1}^N \sum_{n_1=1}^{\infty} e^{-n_1(\beta\omega+2\pi i \frac{a}{N})} \sum_{n_2=1}^{\infty} e^{-n_2(\beta\omega-2\pi i \frac{a}{N})} \\ &= \frac{1}{2\omega} \delta(k_0 + 2\omega) \sum_{n=1}^{\infty} e^{-2n\beta\omega} \\ &= \frac{1}{2\omega} \delta(k_0 + 2\omega) \frac{1}{e^{\beta(2\omega)} - 1}. \end{aligned} \quad (\text{A.15})$$

The a -dependent phase factors cancelled when $n_1 = n_2$ and this gave the non-vanishing contribution. The contribution from the $p_0 = -\omega$ case (A.9) can be calculated in the same way and gives $\frac{1}{2\omega} \delta(k_0 - 2\omega) \frac{1}{e^{\beta(2\omega)} - 1}$. Together with (A.15), this gives the factor $\delta(k_0^2 - (2\omega)^2) \frac{1}{e^{\beta(2\omega)} - 1}$. According to the AdS-CFT dictionary, the scaling dimension two of the operator $\text{tr} \Phi_{(1)}^2$ corresponds to a mass of the closed string state in units of the inverse radius of the AdS, which is ω [4]. Therefore, this is the correct factor for the temperature dependent part of the type-1-type-1 propagator of the *bulk* closed string field theory in the real time formalism.

References

- [1] J. M. Maldacena, “Eternal black holes in Anti-de-Sitter,” JHEP **04** (2003) 021, hep-th/0106112.
- [2] J. M. Maldacena, “The large N limit of superconformal field theories and supergravity,” Adv. Theor. Math. Phys. **2** (1998) 231–252, hep-th/9711200.

- [3] S. W. Hawking and D. N. Page, “THERMODYNAMICS OF BLACK HOLES IN ANTI-DE SITTER SPACE,” *Commun. Math. Phys.* **87** (1983) 577.
- [4] E. Witten, “Anti-de Sitter space and holography,” *Adv. Theor. Math. Phys.* **2** (1998) 253–291, hep-th/9802150.
- [5] E. Witten, “Anti-de Sitter space, thermal phase transition, and confinement in gauge theories,” *Adv. Theor. Math. Phys.* **2** (1998) 505–532, hep-th/9803131.
- [6] T. Matsubara, “A New approach to quantum statistical mechanics,” *Prog. Theor. Phys.* **14** (1955) 351–378.
- [7] G. W. Gibbons and S. W. Hawking, “ACTION INTEGRALS AND PARTITION FUNCTIONS IN QUANTUM GRAVITY,” *Phys. Rev.* **D15** (1977) 2752–2756.
- [8] K. Furuuchi, “From free fields to AdS: Thermal case,” *Phys. Rev.* **D72** (2005) 066009, hep-th/0505148.
- [9] M. Brigante, G. Festuccia, and H. Liu, “Inheritance principle and Non-renormalization theorems at finite temperature,” hep-th/0509117.
- [10] K. Furuuchi, “Large N reductions and holography,” hep-th/0506183.
- [11] Y. Takahasi and H. Umezawa, “Thermo field dynamics,” *Collect. Phenom.* **2** (1975) 55–80.
- [12] H. Umezawa, H. Matsumoto, and M. Tachiki, “THERMO FIELD DYNAMICS AND CONDENSED STATES,”. Amsterdam, Netherlands: North-holland (1982) 591p.
- [13] G. W. Semenoff and H. Umezawa, “FUNCTIONAL METHODS IN THERMO FIELD DYNAMICS: A REAL TIME PERTURBATION THEORY FOR QUANTUM STATISTICAL MECHANICS,” *Nucl. Phys.* **B220** (1983) 196–212.
- [14] A. J. Niemi and G. W. Semenoff, “FINITE TEMPERATURE QUANTUM FIELD THEORY IN MINKOWSKI SPACE,” *Ann. Phys.* **152** (1984) 105.
- [15] A. J. Niemi and G. W. Semenoff, “THERMODYNAMIC CALCULATIONS IN RELATIVISTIC FINITE TEMPERATURE QUANTUM FIELD THEORIES,” *Nucl. Phys.* **B230** (1984) 181.

[16] N. P. Landsman and C. G. van Weert, “REAL AND IMAGINARY TIME FIELD THEORY AT FINITE TEMPERATURE AND DENSITY,” *Phys. Rept.* **145** (1987) 141.

[17] L. Fidkowski, V. Hubeny, M. Kleban, and S. Shenker, “The black hole singularity in AdS/CFT,” *JHEP* **02** (2004) 014, hep-th/0306170.

[18] C. P. Herzog and D. T. Son, “Schwinger-Keldysh propagators from AdS/CFT correspondence,” *JHEP* **03** (2003) 046, hep-th/0212072.

[19] V. Balasubramanian, P. Kraus, A. E. Lawrence, and S. P. Trivedi, “Holographic probes of anti-de Sitter space-times,” *Phys. Rev.* **D59** (1999) 104021, hep-th/9808017.

[20] G. T. Horowitz and D. Marolf, “A new approach to string cosmology,” *JHEP* **07** (1998) 014, hep-th/9805207.

[21] W. Israel, “Thermo field dynamics of black holes,” *Phys. Lett.* **A57** (1976) 107–110.

[22] P. Kraus, H. Ooguri, and S. Shenker, “Inside the horizon with AdS/CFT,” *Phys. Rev.* **D67** (2003) 124022, hep-th/0212277.

[23] S. A. Hartnoll and S. Prem Kumar, “AdS black holes and thermal Yang-Mills correlators,” hep-th/0508092.

[24] O. Aharony, J. Marsano, S. Minwalla, K. Papadodimas, and M. Van Raamsdonk, “The Hagedorn / deconfinement phase transition in weakly coupled large N gauge theories,” *Adv. Theor. Math. Phys.* **8** (2004) 603–696, hep-th/0310285.

[25] O. Aharony, J. Marsano, S. Minwalla, K. Papadodimas, and M. Van Raamsdonk, “A first order deconfinement transition in large N Yang- Mills theory on a small S^{**3} ,” *Phys. Rev.* **D71** (2005) 125018, hep-th/0502149.

[26] B. Sundborg, “The Hagedorn transition, deconfinement and $N = 4$ SYM theory,” *Nucl. Phys.* **B573** (2000) 349–363, hep-th/9908001.

[27] A. M. Polyakov, “Gauge fields and space-time,” *Int. J. Mod. Phys.* **A17S1** (2002) 119–136, hep-th/0110196.

- [28] G. 't Hooft, "A PLANAR DIAGRAM THEORY FOR STRONG INTERACTIONS," *Nucl. Phys.* **B72** (1974) 461.
- [29] R. Gopakumar, "From free fields to AdS," *Phys. Rev.* **D70** (2004) 025009, hep-th/0308184.
- [30] R. Gopakumar, "From free fields to AdS. II," *Phys. Rev.* **D70** (2004) 025010, hep-th/0402063.
- [31] R. Gopakumar, "From free fields to AdS. III," *Phys. Rev.* **D72** (2005) 066008, hep-th/0504229.
- [32] R. Gopakumar, "Free field theory as a string theory?," *Comptes Rendus Physique* **5** (2004) 1111–1119, hep-th/0409233.
- [33] H. Hata and B. Zwiebach, "Developing the covariant Batalin-Vilkovisky approach to string theory," *Ann. Phys.* **229** (1994) 177–216, hep-th/9301097.
- [34] S. S. Gubser, I. R. Klebanov, and A. M. Polyakov, "Gauge theory correlators from non-critical string theory," *Phys. Lett.* **B428** (1998) 105–114, hep-th/9802109.
- [35] Y. Leblanc, "STRING FIELD THEORY AT FINITE TEMPERATURE," *Phys. Rev.* **D36** (1987) 1780.
- [36] D. Berenstein, J. M. Maldacena, and H. Nastase, "Strings in flat space and pp waves from $N = 4$ super Yang Mills," *JHEP* **04** (2002) 013, hep-th/0202021.
- [37] M. C. B. Abdalla, A. L. Gadelha, and D. L. Nedel, "PP-wave light-cone free string field theory at finite temperature," *JHEP* **10** (2005) 063, hep-th/0508195.
- [38] S. D. Mathur, "Is the Polyakov path integral prescription too restrictive?," hep-th/9306090.
- [39] M. C. B. Abdalla, A. L. Gadelha, and D. L. Nedel, "Closed string thermal torus from thermofield dynamics," *Phys. Lett.* **B613** (2005) 213–220, hep-th/0410068.
- [40] B. Sathiapalan, "VORTICES ON THE STRING WORLD SHEET AND CONSTRAINTS ON TORAL COMPACTIFICATION," *Phys. Rev.* **D35** (1987) 3277.

- [41] Y. I. Kogan, “VORTICES ON THE WORLD SHEET AND STRING’S CRITICAL DYNAMICS,” *JETP Lett.* **45** (1987) 709–712.
- [42] J. J. Atick and E. Witten, “THE HAGEDORN TRANSITION AND THE NUMBER OF DEGREES OF FREEDOM OF STRING THEORY,” *Nucl. Phys.* **B310** (1988) 291–334.
- [43] V. Kazakov, I. K. Kostov, and D. Kutasov, “A matrix model for the two-dimensional black hole,” *Nucl. Phys.* **B622** (2002) 141–188, [hep-th/0101011](#).
- [44] S. Kalyana Rama and B. Sathiapalan, “The Hagedorn transition, deconfinement and the AdS/CFT correspondence,” *Mod. Phys. Lett.* **A13** (1998) 3137–3144, [hep-th/9810069](#).
- [45] J. L. F. Barbon and E. Rabinovici, “Closed-string tachyons and the Hagedorn transition in AdS space,” *JHEP* **03** (2002) 057, [hep-th/0112173](#).
- [46] J. L. F. Barbon and E. Rabinovici, “Remarks on black hole instabilities and closed string tachyons,” *Found. Phys.* **33** (2003) 145–165, [hep-th/0211212](#).
- [47] J. McGreevy and E. Silverstein, “The tachyon at the end of the universe,” *JHEP* **08** (2005) 090, [hep-th/0506130](#).
- [48] L. Susskind, L. Thorlacius, and J. Uglum, “The Stretched horizon and black hole complementarity,” *Phys. Rev.* **D48** (1993) 3743–3761, [hep-th/9306069](#).
- [49] J. B. Hartle and S. W. Hawking, “PATH INTEGRAL DERIVATION OF BLACK HOLE RADIANCE,” *Phys. Rev.* **D13** (1976) 2188–2203.
- [50] J. B. Hartle and S. W. Hawking, “WAVE FUNCTION OF THE UNIVERSE,” *Phys. Rev.* **D28** (1983) 2960–2975.
- [51] A. M. Polyakov, “THERMAL PROPERTIES OF GAUGE FIELDS AND QUARK LIBERATION,” *Phys. Lett.* **B72** (1978) 477–480.
- [52] S. W. Hawking, “BREAKDOWN OF PREDICTABILITY IN GRAVITATIONAL COLLAPSE,” *Phys. Rev.* **D14** (1976) 2460–2473.

- [53] J. S. Schwinger, “Brownian motion of a quantum oscillator,” *J. Math. Phys.* **2** (1961) 407–432.
- [54] L. V. Keldysh, “Diagram technique for nonequilibrium processes,” *Zh. Eksp. Teor. Fiz.* **47** (1964) 1515–1527.
- [55] S. D. Mathur, A. Saxena, and Y. K. Srivastava, “Constructing ‘hair’ for the three charge hole,” *Nucl. Phys.* **B680** (2004) 415–449, hep-th/0311092.
- [56] G. Festuccia and H. Liu, “Excursions beyond the horizon: Black hole singularities in Yang-Mills theories. I,” hep-th/0506202.
- [57] S. W. Hawking, “Particle creation by black holes,” *Commun. Math. Phys.* **43** (1975) 199–220.
- [58] D. T. Son and A. O. Starinets, “Minkowski-space correlators in AdS/CFT correspondence: Recipe and applications,” *JHEP* **09** (2002) 042, hep-th/0205051.